J. metamorphic Geol., 2004, **22,** 671–687 doi:10.1111/j.1525-1314.2004.00541.x

The fate of subducted continental margins: Two-stage exhumation of the high-pressure to ultrahigh-pressure Western Gneiss Region, Norway

E. O. WALSH* AND B. R. HACKER
Department of Geological Sciences, University of California, Santa Barbara, CA 93106-9630, USA (walshe@union.edu)

ABSTRACT Thermobarometry suggests that ultrahigh-pressure (UHP) to high-pressure (HP) rocks across the Western Gneiss Region ponded at the Moho following as much as 100 km of exhumation through the mantle and before exhumation to the upper crust. Eclogite across the *c.* 22 000 km^2 study area records minimum pressures of *c.* 8–18 kbar and temperatures of *c.* 650–780 °C. One orthopyroxene eclogite yields an UHP of *c.* 28.5 kbar, and evidence of former coesite has been found *c.* 50 km farther east than previously known. Despite this widespread evidence of UHP to HP, thermobarometry of metapelite and garnet amphibolite samples reveals a surprisingly uniform 'supra-Barrovian' amphibolite-facies overprint at *c.* 11 kbar and *c.* 650–750 °C across the entire area. Chemical zoning analysis suggests that garnet in these samples grew during heating and decompression, presumably during the amphibolite-facies event. These data indicate that the Norwegian UHP/HP province was exhumed from mantle depths of *c.* 150 km to lower crustal depths, where it stalled and underwent a profound high-temperature overprint. The ubiquity of late-stage supra-Barrovian metamorphic overprints suggests that large-scale, collisional UHP terranes routinely stall at the continental Moho where diminishing body forces are exceeded by boundary forces. Significant portions of the middle or lower crust worldwide may be formed from UHP terranes that were arrested at the Moho and never underwent their final stage of exhumation.

Key words: exhumation; supra-Barrovian overprint; thermobarometry; ultrahigh-pressure rocks; Western Gneiss Region.

INTRODUCTION

What is the fate of subducted continental crust? How much is recycled into the mantle, how much is returned to the crust, and how much is exhumed to Earth's surface? What are the mechanisms and kinematics of these processes? This paper proposes that the high-pressure (HP) and ultrahigh-pressure (UHP) rocks in the Western Gneiss Region (WGR) of Norway were not exhumed from UHP depths in a single stage, but rather, stalled and re-equilibrated at the Moho after exhumation through the mantle. Subsequent crustal extension then carried these rocks to Earth's surface. This two-stage process implies that (i) exhumation of UHP/HP rocks may often be incomplete, (ii) the middle or lower continental crust worldwide may include incompletely exhumed UHP/HP terranes, and (iii) the surficial record of UHP rocks may lead to a significant underestimate of the prevalence of UHP processes in Earth's evolution.

The UHP–HP terrane in the WGR of Norway (Fig. 1) is one of the world's largest, covering $>30\,000$ km^2. Like other well-known UHP terranes, it is composed almost exclusively of continental rocks that reached UHP – as high as 40 kbar – as demonstrated by the presence of coesite, quartz pseudomorphs replacing coesite, and diamond (Cuthbert *et al.*, 2000; Terry *et al.*, 2000). Garnet peridotite within the UHP terrane contains rare former majoritic garnet, which points to pressures as high as 60–80 kbar (van Roermund *et al.*, 2001). A thermobarometric study of a 220×100 km E–W transect across the UHP/HP terrane of southwestern Norway (Fig. 2) was conducted to increase understanding of the exhumation of this archetypal UHP terrane. Specifically, the exhumation path was assessed through study of: (i) the *P–T* histories of basement rocks in comparison with allochthonous rocks; (ii) the *P–T* histories of different rock types, including metapelite, garnet amphibolite and eclogite; and (iii) the areal distribution of eclogite and its relationship to the host rocks.

GEOLOGICAL SETTING

Paleomagnetic data suggest that the Caledonian orogen in Scandinavia formed from the mid-Silurian collision of Baltica and Laurentia (Torsvik, 1998). The orogen includes a stack of nappes – grouped into Lower, Middle, Upper, and Uppermost Allochthons

**Present address*: E. O. Walsh, Geology Department, Union College, Schenectady, NY 12308, USA.

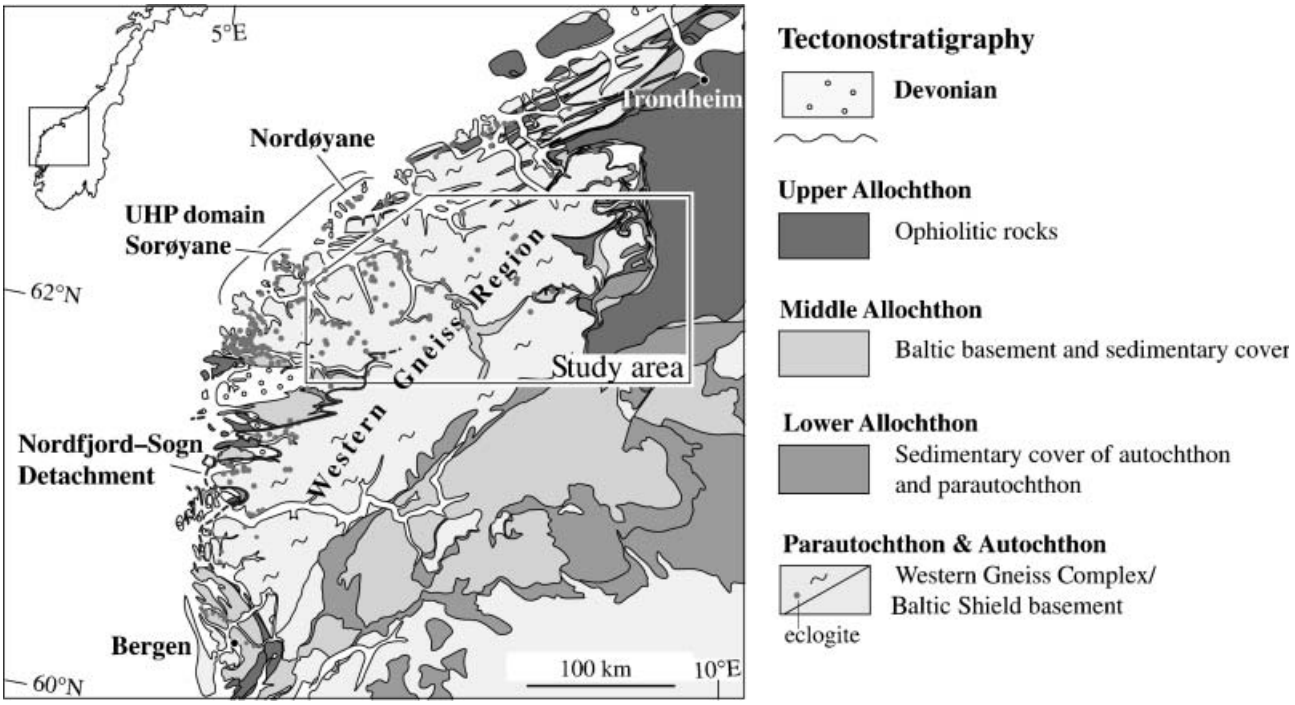

Fig. 1. Geology of southwestern Norway, emphasizing the ultrahigh-pressure to high-pressure terrane (see 'eclogites') of the Western Gneiss Region.

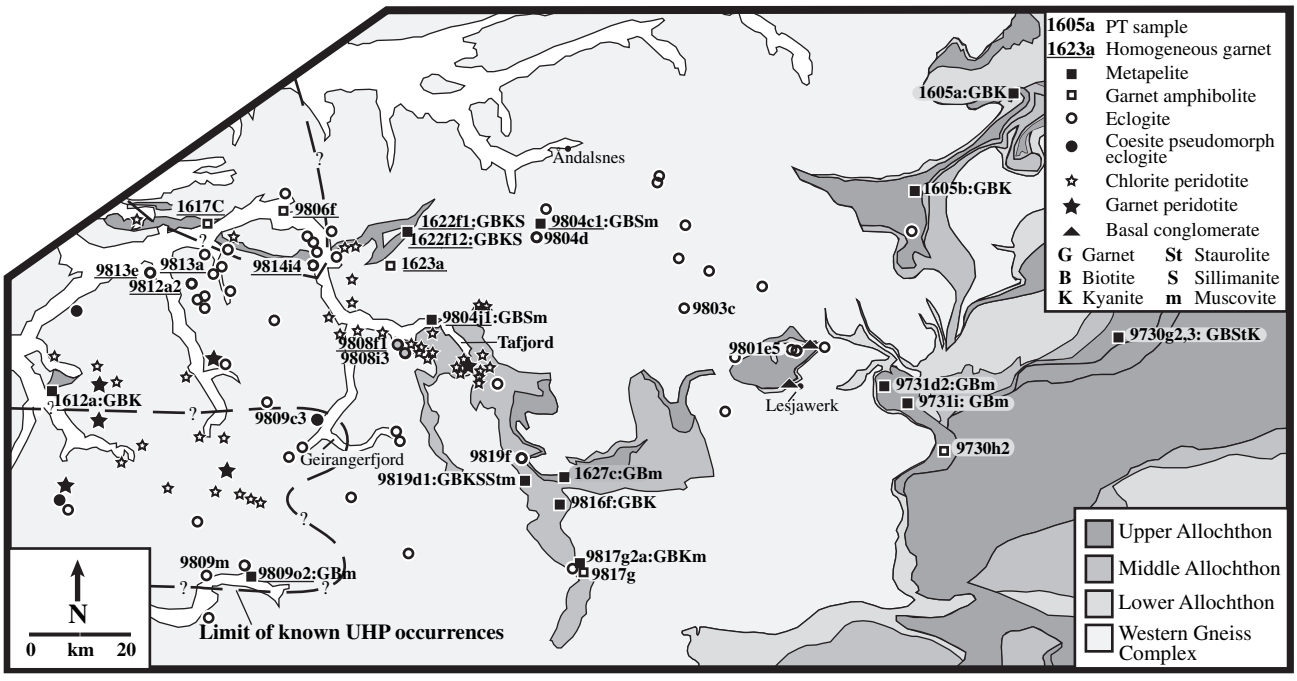

Fig. 2. Geological map of the study area showing the locations of *P–T* samples, eclogite and peridotite. Eclogite and peridotite localities from this study, Medaris (1984); Ajebli (1995), and Cuthbert *et al.* (2000). The dashed line shows the limit of known UHP rocks (Cuthbert *et al.*, 2000; this study).

(Fig. 3) – that were emplaced southeastward onto the autochthonous Precambrian Baltica basement from *c.* 425–400 Ma (Roberts & Gee, 1985; Hacker & Gans, in press). These nappes are best exposed and least metamorphosed in western Sweden and eastern Norway, east of the WGR. The autochthon consists chiefly

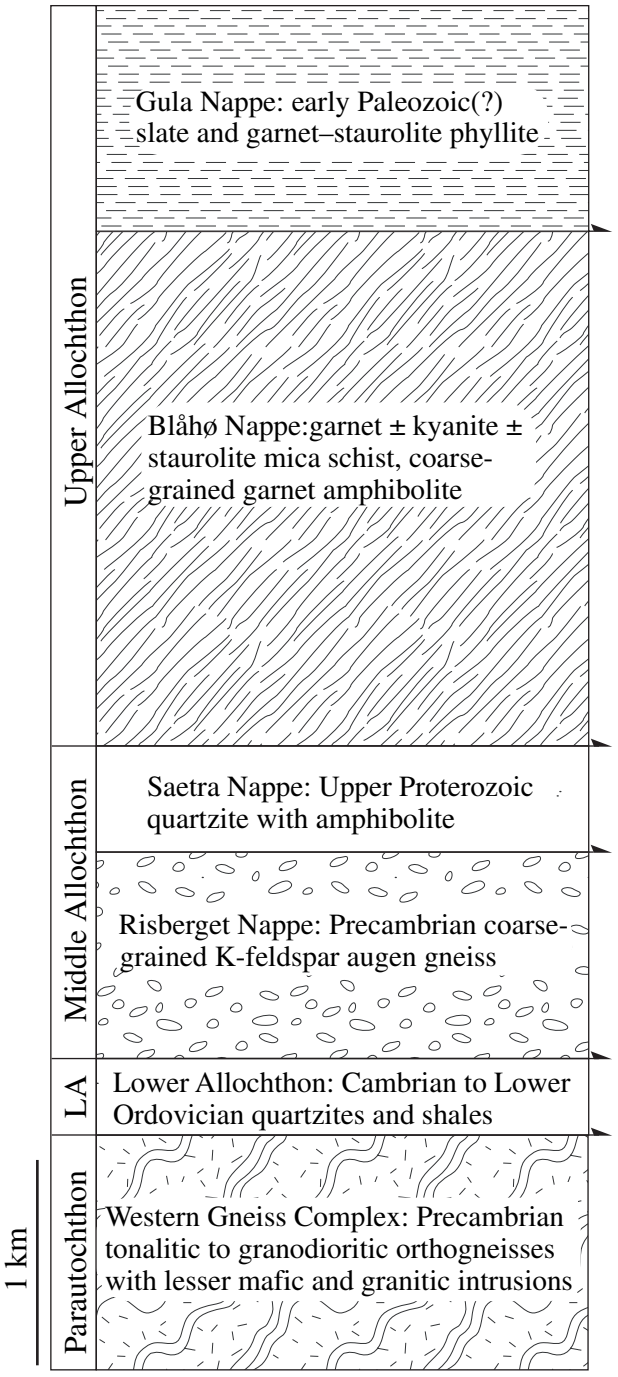

Fig. 3. Tectono-stratigraphic column of allochthonous units with representative thicknesses. Data compiled from Gee (1975), Guezou (1978), Gee & Zachrisson (1979), Kollung (1984), Bryhni & Sturt (1985), Gee *et al.* (1985), Kollung (1990), and Lutro *et al.* (1997).

of *c.* 1700–950 Ma tonalitic to granodioritic orthogneiss (Corfu, 1980; Schärer, 1980; Tucker *et al.*, 1990). West of the autochthon, and separated from it by a 20-km wide section of overlying nappes, is the compositionally and temporally similar Western Gneiss Complex (WGC) that contains numerous UHP and HP eclogite and peridotite bodies. (Note the distinction between the WGC, a rock unit, and the WGR, an area).

Crystalline rocks and their Lower Ordovician sedimentary cover that have been thrust over the autochthon comprise the Lower Allochthon (Bryhni & Sturt, 1985). The Middle Allochthon consists of Precambrian crystalline rocks covered by Upper Proterozoic feldspathic quartzite that is locally intruded by dolerite dykes (Svenningsen, 2001), and is interpreted to have been part of the Baltica continental margin that lay outboard (west) of the WGC (Milnes *et al.*, 1997). The lower unit of the Upper Allochthon, the Blåhø Nappe, is also interpreted to have been derived from outboard Baltica (Gee *et al.*, 1985; Lutro *et al.*, 1997), whereas the upper unit, the Gula and Støren Nappes, is an assemblage of Late Cambrian to Early Silurian oceanic sedimentary and ophiolitic rocks (summary in Hacker & Gans, in press).

STUDY AREA

The rocks in a 100-km wide transect extending *c.* 220 km from the coastal UHP domain eastward to the stack of Caledonian allochthons were the focus of this study. The study area is underlain principally by the WGC but also contains thin sheets of allochthonous rocks that have been correlated with the classic nappe sequence, discussed above, in the east. The correlations and terminology used here are that of Krill (1985); Robinson (1995), and Lutro *et al.* (1997), who called these allochthonous rocks the Risberget, Saetra, and Blåhø/Gula Nappes and correlated them with the Tännäs, Särv and Seve Nappes of the Swedish Caledonides, respectively (Fig. 3).

Across the study area, the WGC is largely composed of isoclinally folded, variably banded quartz + biotite + plagioclase ± K-feldspar ± muscovite ± garnet ± amphibole gneiss containing volumetrically less significant, deformed, quartzofeldspathic anatectites, granitic intrusions and pegmatitic dykes. Sheets and lenses of mafic meta-igneous rock comprise a few percent of the WGC and range from weakly metamorphosed gabbro to amphibolite to eclogite; eclogite is most prevalent in the northwestern portion of the study area and rare in the east (Fig. 2). Capping the WGC is a rarely exposed feldspathic and locally micaceous quartzite of the Lower Allochthon. The quartzite ranges from massive to banded and includes a basal quartz-pebble conglomerate at two localities (Fig. 2).

The Middle Allochthon in the northern portion of the study area is composed of the Risberget and Saetra Nappes. The Risberget Nappe mainly includes megacrystic, K-feldspar augen gneiss with a fine-grained, biotite-rich matrix that grades with increasing deformation into variably mylonitic, fine-grained, laminated biotite–quartz–plagioclase gneiss in which the feldspar

augen have been destroyed. Lesser volumes of metagabbro, anorthosite, amphibolite, equigranular orthogneiss and local eclogite are commonly associated with the augen gneiss. Structurally overlying the Risberget Nappe is the Saetra Nappe: strongly laminated, feldspathic and micaceous quartzite associated with amphibolite. In the southwestern portion of the area, the Risberget Nappe is less abundant, and epidote–biotite gneiss, muscovite gneiss, garnet–muscovite–quartz gneiss and anorthosite are the typical Middle Allochthon rocks (Strand, 1969; Brueckner, 1977; Bryhni & Sturt, 1985).

The Upper Allochthon in the study area is represented by the Blåhø and Gula Nappes. The Blåhø Nappe is dominated by garnet ± kyanite ± staurolite mica schist and coarse-grained garnet amphibolite with plagioclase-rich laminae; it also includes biotite schist, feldspathic gneiss, muscovite–quartz gneiss, retrogressed eclogite pods and rare carbonate layers. The Blåhø Nappe is spatially associated with the Risberget Nappe across the study area. The Gula Nappe, exposed at the eastern edge of the transect, consists of fine-grained slate and garnet–staurolite phyllite.

Eclogite exists in the allochthons and in the autochthon. It is distributed across the study area but is concentrated in the northwest and notably rare in the east. It mainly forms lenses or pods, many of which are surrounded by a rind of retrograde garnet amphibolite. Eclogite containing known coesite or diamond occurs within a 5000 km^2 domain of coastal Norway, located just off the western edge of Fig. 2. No recognized structure separates the UHP rocks from the HP rocks, suggesting that the boundary is kinetic, gradational or overprinted (Root *et al.*, in review). Zircon from eclogite collected across the study area yield Precambrian cores and Caledonian (*c.* 440–400 Ma) HP to UHP rims (our data, unpubl. results; Root *et al.*, in press). Orthopyroxene eclogite – or garnet websterite – occurs in the northwest. Fe-rich crustal peridotite and Mg–Cr mantle peridotite is scattered throughout the western part of the study area (Carswell *et al.*, 1983, 1985; Cuthbert *et al.*, 2000), and although much of the mantle peridotite has been retrogressed to chlorite peridotite, some bodies still retain garnet (Medaris, 1984).

PETROLOGICAL OBSERVATIONS

From 240 samples collected during structural and petrological fieldwork, 32 samples were selected for thermobarometry and *P–T* path modelling. Efforts were focused on metapelite, garnet amphibolite and eclogite that contain low-variance parageneses and were only weakly retrogressed.

The typical metapelite mineral assemblage in the study area is garnet + biotite + plagioclase ($An_{15–47}$) + quartz ± kyanite/sillimanite ± muscovite ± staurolite (Table 1), characteristic of amphibolite-facies temperatures and pressures and a Barrovian metamorphic series. Common accessory minerals include zircon, monazite, apatite, rutile, titanite, calcite, ilmenite, hematite, zoisite, and epidote (Table 1). Inclusions in garnet consist mainly of quartz, biotite, ilmenite, rutile, monazite, and zircon. Inclusions of muscovite are present in garnet from five samples; inclusions of plagioclase are present in garnet from six samples, and sillimanite is included in garnet in sample 9804c1. Garnet radii range greatly from *c.* 450 to 5000 μm with an average of *c.* 2000 μm; whereas most metapelite garnet retains prograde zoning, the three smallest garnet grains (< 1000 μm in radius) are homogeneous. Typical retrograde reactions in the metapelite samples include the breakdown of phengite to biotite + plagioclase and the breakdown of garnet to biotite + plagioclase or chlorite.

Metapelite containing kyanite is restricted to allochthonous rocks in the southern portion of the study area (with the exception of 1605a & 1605b) and is interspersed with metapelite lacking aluminium silicate, implying a bulk compositional control (see Fig. 2). Basement metapelite contains sillimanite instead of kyanite, and fibrolite replaces kyanite in one allochthon sample (9819d1) in the central part of the study area. Sillimanite is limited to the north-central part of the study area. Staurolite is rare, occurring at three localities (9730g2, 9730g3, and 9819d1) that also contain kyanite. Two of the easternmost samples (9730g2 and 9730g3) contain paragonite. Muscovite is found in three of the rocks containing sillimanite but occurs with kyanite at only one locality in the centre of the study area (9819d1).

Amphibolite is pervasive across the study area. The typical mineral assemblage for garnet amphibolite is garnet + amphibole + plagioclase + quartz ± biotite ± muscovite, and accessory minerals include titanite, ilmenite, calcite, rutile, epidote, and apatite (Table 1). The anorthite content of plagioclase generally increases westward from $An_{14–27}$ (9730h2) to $An_{42–87}$ (1617c), and amphibole compositions are solid solutions of predominantly (ferro-)pargasite, tschermakite and magnesio-hornblende. Typical inclusions in garnet are quartz and rutile, along with amphibole, biotite, opaque minerals, titanite, epidote, apatite, plagioclase, calcite, and clinozoisite. Grains of garnet range in radius from *c.* 800 to 2300 μm with an average of *c.* 1500 μm; all garnet records prograde zoning, with the exception of the two samples containing the smallest garnet grains. Most samples exhibit partial plagioclase decomposition to sericite and breakdown of garnet to biotite + plagioclase + amphibole or to ilmenite + amphibole + plagioclase.

Eclogite located across the study area, in the basement and in the allochthons, is typically highly retrogressed. The peak mineral assemblage ranged from garnet + quartz/coesite + omphacite ± phengite ± amphibole to garnet + omphacite ± biotite ± orthopyroxene ± amphibole, but at present, most grains are partially to wholly converted to fine-grained

Table 1. Sample mineralogy.

	Major phases											Minor phases											
Sample no.	Grt	Bt	Ms	Pl	Qtz	St	Ky	Sil	Am[b]	Cpx	Opx	Zrn	Mnz	Aln	Opq[c]	Ap	Ep/Zo	Rt	Ttn	Cal	Chl	Tur	Kfs	Estimated garnet resorption[a]
9730g2	x	x	Pg	x	x	x	x					x			x	x			x		bp			1.7
9730g3	x	x	Pg	x	x	x	x						x					x		x	bp			0.0
9731d2	x	x	x	x	x								x			x		x		x		x		0.1
9731i	x	bp	x	x	x							x		x		x		x						9.0
9804c1	x	x	x	x	x			inc					x		x	x							x	5.2
9804j1	x	x	x	x	x			x					x		x	x					bp			28.9
9809o2	x	x	x	x	x										x	x	x	x	x				x	5.8
9816f	x	x		x	x		x					x			x		x	x			bp			13.6
9817g2a	x	x		x	x		x								x	x		x			bp			6.3
9819d1	x	x	x	x	x	x	x	r							x	x		x						>11.3
1605a	x	x		x	x		x					x				x		x						7.3
1605b	x	x		x	x		x																	1.9
1612a	x	x		x	x		x									x								4.1
1622f1	x	x		x	x		x					x									bp		x	19.6
1622f2	x	x		x	x		x											x					x	1.5
1627c	x	x	x	x	x										x	x		x						4.4
9730h2	x	x	x	x	x				x						x	x	x		x	x				
9731d1	x	x	x	x	x				x						x	x		x	x	x	bp			
9806f1	x	x		x	x				x						x	x	x							
9817g	x	x		x	x				x						x	x		x	x	x				
1617c1	x	x		x	x				x						x			x						
1623a	x	x		x	x				x			x			x			x						
9801e5	x	x		x	x				bp	sym					x	x	x	x						
9804d	x	bp		bp	x					sym		x			x	x	x		x					
9803c	x	bp?		bp					x	sym					sym			x	x					
9808f1	x	sym		bp	x				sym	sym					x	x	x	x		x				
98081i3	x			bp	x				bp	sym					x	x		x						
9809m	x	x	x		x				bp	x					x	x	x	x		x				
9812a2	x	x		bp	x				bp	sym					x	x								
9813a	x			bp	x				bp	rods								x						
9813e	x	bp		bp	x					x					x	x		x		x				
9814i4	x	x							x	x	x													
9819f	x	bp		bp	x				bp	sym					x	x	x	x						

Mineral abbreviations after Kretz (1983) and Bucher & Frey (1994).
[a]Estimated garnet resorption for pelites – recorded as % of garnet size; method after Kohn & Spear (2000).
[b]Undifferentiated amphibole.
[c]Undifferentiated opaque minerals.
bp, mineral present only as breakdown product; inc, mineral found only as inclusion; r, sillimanite replacing kyanite, in equilibrium with garnet rim; rods, silica rods present in clinopyroxene; sym, mineral present only as part of symplectite.

symplectites such as clinopyroxene + plagioclase from omphacite, amphibole + plagioclase from clinopyroxene, and biotite + plagioclase from phengite. Accessory minerals include epidote, clinozoisite, apatite, rutile, titanite, opaque minerals and calcite (Table 1); there are no apparent mineralogical differences between basement eclogite and allochthon eclogite. Inclusions in garnet are many and varied: rutile, titanite, amphibole, quartz, zircon, biotite, muscovite, zoisite, plagioclase, clinopyroxene, apatite, and in one instance, omphacite. Inclusions of rutile in garnet are either exsolved rods or anhedral grains similar in size and morphology to matrix grains. Garnet grains range in radius from *c*. 200 to 2000 μm with an average of *c*. 1000 μm.

Omphacite survives in three samples (9809m, 9813a, and 9813e) and yields calculated jadeite contents of jd_{37-51}. Inclusions of phengite in garnet are present in one sample in the east (9803c), but matrix phengite has been replaced in all samples by coarse biotite–plagioclase symplectites. All plagioclase is retrograde. Eclogite from the central part of the study area around Geirangerfjord (Fig. 2) displays particularly well-preserved, coarse-grained (partially annealed) symplectites

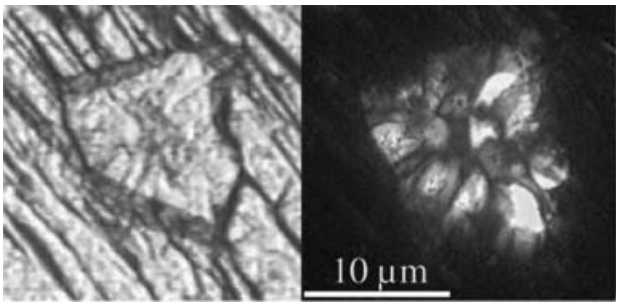

Fig. 4. Palisade-textured, polycrystalline quartz inclusion in a garnet from eclogite sample 9809c3, shown in plain and cross-polarized light.

replacing almost every high-pressure mineral. Peridotite exists chiefly in the western half of the area; garnet peridotite tends to be surrounded by a rind of retrogressed chlorite peridotite. Orthopyroxene is present at locality 9814i4, and one garnet grain from sample 9809c3 contains an inclusion of palisade-textured, polycrystalline quartz that, based on these textures (Hacker & Peacock, 1995), replaced coesite (Fig. 4). Sample 9813e contains silica rods within

clinopyroxene, implying exsolution from a more silica-rich precursor (Zhang & Liou, 2000); silica rods are absent from all other eclogite samples.

THERMOBAROMETRY

Polished thin sections from these 32 samples were analysed with a 5-wavelength-dispersive-spectrometer Cameca SX-50 electron microprobe operated at 15 kV accelerating voltage and 15 nA sample current. X-ray element maps were made of one or two of the largest garnet grains in each sample to determine garnet growth patterns. These garnet grains were then analysed, along with adjacent grains of biotite, plagioclase, amphibole or muscovite, and matrix grains of biotite, plagioclase, amphibole, muscovite or omphacite distant from the garnet grains (Tables 2–4). Clinopyroxene + plagioclase symplectites were also analysed.

Table 2. Electron microprobe analyses for metapelite samples.

	SiO_2	Al_2O_3	TiO_2	FeO*	Cr_2O_3	MnO	MgO	CaO	Na_2O	K_2O	Total	#O	Si	Al	Ti	Fe	Cr	Mn	Mg	Ca	Na	K	Total	X_{an}	Fe#	X_{grs}	X_{sps}
9730g2 Grt	37.10	21.15	0.09	32.30	<	0.52	3.53	6.01	<	<	100.7	12	2.95	1.98	0.01	2.15	0.00	0.04	0.42	0.51	0.00	0.00	8.05		0.84	0.16	0.01
9730g2 Bt	33.99	19.11	1.06	20.58	<	0.06	11.86	<	<	7.08	93.7	11	2.62	1.74	0.06	1.33	0.00	0.00	1.36	0.00	0.00	0.70	7.80		0.49		
9730g2 Pl	63.38	23.39	<	0.28	<	<	<	4.52	9.07	0.05	100.7	8	2.79	1.21	0.00	0.01	0.00	0.00	0.00	0.21	0.77	0.00	5.00	0.22			
9730g2 St	27.89	54.00	0.71	13.01	0.09	0.10	1.71	<	0.32	<	97.8	23	3.86	8.81	0.07	1.51	0.01	0.01	0.35	0.00	0.08	0.00	14.70		0.81		
9730g3 Grt	37.84	21.50	<	32.30	<	0.35	3.98	4.84	<	<	100.8	12	2.99	2.00	0.00	2.13	0.00	0.02	0.47	0.41	0.00	0.00	8.02		0.82	0.14	0.01
9730g3 Bt	35.48	18.63	1.62	20.52	0.06	<	9.90	<	0.15	8.66	95.0	11	2.71	1.68	0.09	1.31	0.00	0.00	1.13	0.00	0.02	0.84	7.78		0.54		
9730g3 Pl	60.15	25.30	<	0.08	<	<	<	6.99	7.52	0.07	100.1	8	2.67	1.33	0.00	0.00	0.00	0.00	0.00	0.33	0.65	0.00	4.98	0.34			
9730g3 St	26.71	52.50	0.71	11.75	0.06	0.06	0.92	<	<	<	92.7	23	3.87	8.97	0.08	1.43	0.01	0.01	0.20	0.00	0.00	0.00	14.57		0.88		
1605a Grt	38.14	21.45	<	29.51	<	0.14	5.25	5.74	<	<	100.2	12	2.99	1.98	0.00	1.94	0.00	0.01	0.61	0.48	0.00	0.00	8.01		0.76	0.16	0.00
1605a Bt	36.69	18.92	1.53	17.70	0.06	0.08	12.60	0.07	0.12	8.30	96.1	11	2.72	1.65	0.09	1.10	0.00	0.01	1.39	0.01	0.02	0.79	7.77		0.44		
1605a Pl	59.15	26.16	<	0.35	<	<	<	7.95	7.16	0.05	100.8	8	2.62	1.37	0.00	0.01	0.00	0.00	0.00	0.38	0.62	0.00	5.00	0.38			
1605b Grt	38.10	21.76	0.05	29.59	<	0.05	5.19	5.80	<	<	100.5	12	2.98	2.01	0.00	1.93	0.00	0.00	0.60	0.49	0.00	0.00	8.02		0.76	0.16	0.00
1605b Bt	37.67	20.78	0.81	13.13	0.06	<	14.23	0.07	0.28	8.91	95.9	11	2.73	1.78	0.04	0.80	0.00	0.00	1.54	0.01	0.04	0.83	7.77		0.34		
1605b Pl	60.44	25.69	<	0.10	<	<	<	6.90	7.62	0.10	100.9	8	2.67	1.34	0.00	0.00	0.00	0.00	0.00	0.33	0.65	0.01	4.99	0.33			
9731I Grt	37.20	21.10	<	33.89	0.05	0.59	3.17	4.57	<	<	100.6	12	2.97	1.99	0.00	2.26	0.00	0.04	0.38	0.39	0.00	0.00	8.03		0.86	0.13	0.01
9731I Bt	34.17	18.15	3.68	18.45	0.10	0.06	10.25	<	<	9.43	94.3	11	2.63	1.65	0.21	1.19	0.01	0.00	1.18	0.00	0.00	0.93	7.79		0.50		
9731I Pl	63.68	22.42	<	<	<	<	<	4.21	8.95	0.15	99.5	8	2.83	1.17	0.00	0.00	0.00	0.00	0.00	0.20	0.77	0.01	4.97	0.20			
9731I Ms	47.73	30.96	0.67	1.96	<	<	2.11	<	0.49	10.59	94.5	11	3.22	2.46	0.03	0.11	0.00	0.00	0.21	0.00	0.06	0.91	7.01				
9731d2 Grt	37.63	21.28	<	31.35	0.05	1.01	3.33	5.74	<	<	100.4	12	2.90	1.99	0.00	2.08	0.00	0.07	0.39	0.49	0.00	0.00	7.92		0.84	0.16	0.02
9731d2 Bt	35.34	17.27	2.72	19.34	<	0.16	10.27	<	0.11	9.20	94.4	11	2.72	1.57	0.16	1.25	0.00	0.01	1.18	0.00	0.02	0.90	7.80		0.51		
9731d2 Pl	61.09	24.12	<	0.27	<	<	<	6.27	7.99	0.08	99.8	8	2.72	1.27	0.00	0.01	0.00	0.00	0.00	0.30	0.69	0.00	4.99	0.30			
9731d2 Ms	45.91	34.05	0.40	1.45	<	0.05	0.76	<	0.78	9.74	93.1	11	3.12	2.73	0.02	0.08	0.00	0.00	0.08	0.00	0.10	0.84	6.97				
9817g2a Grt	37.91	21.52	0.06	31.47	<	0.66	3.99	5.66	<	<	101.3	12	2.98	1.99	0.00	2.07	0.00	0.04	0.47	0.48	0.00	0.00	8.02		0.82	0.16	0.01
9817g2a Bt	37.02	16.74	1.86	14.35	0.05	0.07	14.15	<	<	9.70	93.9	11	2.79	1.49	0.11	0.91	0.00	0.01	1.59	0.00	0.00	0.93	7.82		0.36		
9817g2a Pl	60.86	24.48	<	<	<	<	<	6.32	8.13	0.12	99.9	8	2.71	1.28	0.00	0.00	0.00	0.00	0.00	0.30	0.70	0.01	5.00	0.30			
1627c Grt	37.54	21.03	0.06	32.62	<	1.84	3.33	4.75	<	<	101.2	12	2.98	1.97	0.00	2.16	0.00	0.12	0.39	0.40	0.00	0.00	8.03		0.85	0.13	0.04
1627c Bt	33.95	18.62	2.01	18.60	<	0.17	9.76	0.06	0.07	9.02	92.3	11	2.67	1.73	0.12	1.22	0.00	0.01	1.14	0.01	0.01	0.91	7.81		0.52		
1627c Pl	61.43	24.23	<	<	<	<	<	5.92	8.11	0.17	99.9	8	2.73	1.27	0.00	0.00	0.00	0.00	0.00	0.28	0.70	0.01	4.99	0.28			
1627c Ms	44.26	33.55	0.98	3.15	<	<	0.96	<	0.66	10.15	93.7	11	3.03	2.71	0.50	0.18	0.00	0.00	0.10	0.00	0.09	0.89	7.50				
9816f Grt	37.57	21.71	<	28.52	<	0.33	3.97	8.57	<	<	100.7	12	2.95	2.01	0.00	1.87	0.00	0.02	0.46	0.72	0.00	0.00	8.04		0.80	0.23	0.01
9816f Bt	35.85	17.06	1.92	15.30	0.09	<	14.76	0.08	0.06	8.83	94.0	11	2.71	1.52	0.11	0.97	0.01	0.00	1.66	0.01	0.01	0.85	7.85		0.37		
9816f Pl	55.35	27.60	<	0.21	<	<	<	9.69	6.13	0.06	99.0	8	2.52	1.48	0.00	0.01	0.00	0.00	0.00	0.47	0.54	0.00	5.02	0.46			
9804c1 Grt	37.46	20.77	<	29.26	<	6.45	4.21	1.96	<	<	100.1	12	3.00	1.96	0.00	1.96	0.00	0.44	0.50	0.17	0.00	0.00	8.02		0.80	0.05	0.14
9804c1 Bt	34.24	16.59	3.15	19.76	<	0.50	9.65	<	<	9.41	93.3	11	2.69	1.54	0.19	1.30	0.00	0.03	1.13	0.00	0.00	0.94	7.83		0.53		
9804c1 Pl	57.40	26.25	<	0.10	<	<	<	8.91	6.54	0.14	99.3	8	2.59	1.40	0.00	0.00	0.00	0.00	0.00	0.43	0.57	0.01	5.00	0.43			
9804c1 Ms	45.17	34.64	0.50	3.75	<	<	0.58	<	0.29	10.20	95.1	11	3.05	2.75	0.03	0.21	0.00	0.00	0.06	0.00	0.04	0.88	7.01				
9819d1 Grt	36.32	21.38	<	30.74	<	0.45	3.18	6.75	<	<	98.8	12	2.93	2.04	0.00	2.08	0.00	0.03	0.38	0.58	0.00	0.00	8.05		0.84	0.19	0.01
9819d1 Bt	33.10	19.15	1.89	18.15	<	0.08	12.37	<	0.08	9.23	94.1	11	2.55	1.74	0.11	1.17	0.00	0.01	1.42	0.00	0.01	0.91	7.93		0.45		
9819d1 Pl	62.77	23.68	<	0.11	<	<	<	5.02	8.54	0.20	100.3	8	2.77	1.23	0.00	0.00	0.00	0.00	0.00	0.24	0.73	0.01	4.99	0.24			
9819d1 Ms	47.38	32.97	0.39	2.97	<	<	0.93	0.05	0.54	8.22	93.5	11	3.19	2.62	0.02	0.17	0.00	0.00	0.09	0.00	0.07	0.71	6.87				
9804j1 Grt	38.16	21.64	<	29.93	<	3.25	6.18	2.10	<	<	101.3	12	2.98	1.99	0.00	1.95	0.00	0.22	0.72	0.18	0.00	0.00	8.03		0.73	0.06	0.07
9804j1 Bt	35.33	19.37	0.97	17.94	<	0.15	11.43	<	0.14	9.46	94.8	11	2.69	1.74	0.06	1.14	0.00	0.01	1.30	0.00	0.02	0.92	7.86		0.47		
9804j1 Pl	63.12	23.50	<	<	<	<	<	4.91	8.62	0.15	100.3	8	2.78	1.22	0.00	0.00	0.00	0.00	0.00	0.23	0.74	0.01	4.98	0.24			
9804j1 Ms	46.11	32.20	0.70	2.85	<	<	1.02	<	0.74	9.88	93.6	11	3.15	2.59	0.04	0.16	0.00	0.00	0.10	0.00	0.10	0.86	7.00				
1622f1 Grt	37.42	21.81	<	29.30	<	0.60	7.42	3.31	<	<	99.9	12	2.93	2.02	0.00	1.92	0.00	0.04	0.87	0.28	0.00	0.00	8.06		0.69	0.09	0.01
1622f1 Bt	34.69	17.76	3.22	15.00	0.12	0.08	13.75	<	0.05	9.24	93.9	11	2.64	1.59	0.18	0.95	0.01	0.01	1.56	0.00	0.01	0.90	7.83		0.38		
1622f1 Pl	57.64	26.28	<	0.55	<	<	<	8.09	6.81	<	99.4	8	2.60	1.40	0.00	0.02	0.00	0.00	0.00	0.39	0.60	0.00	5.00	0.40			
1622f2 Grt	38.49	22.10	<	27.28	<	0.84	7.60	4.18	<	<	100.5	12	2.97	2.01	0.00	1.76	0.00	0.06	0.88	0.35	0.00	0.00	8.02		0.67	0.11	0.02
1622f2 Bt	36.80	18.27	2.16	13.44	0.12	0.05	14.56	<	0.30	9.54	95.2	11	2.72	1.59	0.12	0.83	0.01	0.00	1.61	0.00	0.04	0.90	7.83		0.34		
1622f2 Pl	59.33	26.31	<	0.41	<	<	<	7.72	7.02	0.05	100.8	8	2.63	1.37	0.00	0.02	0.00	0.00	0.00	0.37	0.60	0.00	4.99	0.38			
9809o2 Grt	36.86	20.81	<	28.69	<	9.25	2.33	2.39	<	<	100.3	12	2.98	1.98	0.00	1.94	0.00	0.63	0.28	0.21	0.00	0.00	8.03		0.87	0.07	0.21
9809o2 Bt	34.70	16.33	2.08	22.80	<	0.56	8.39	<	<	9.71	94.6	11	2.73	1.52	0.12	1.50	0.00	0.04	0.99	0.00	0.00	0.98	7.87		0.60		
9809o2 Pl	60.63	24.94	<	0.12	<	<	<	6.83	7.56	0.22	100.3	8	2.69	1.31	0.00	0.00	0.00	0.00	0.00	0.33	0.65	0.01	4.99	0.33			
9809o2 Ms	45.34	32.34	<	3.68	<	0.05	0.93	<	0.23	10.68	93.3	11	3.13	2.63	0.00	0.21	0.00	0.00	0.10	0.00	0.03	0.94	7.04				
1612a Grt	38.27	21.77	0.04	28.08	<	0.30	7.91	4.06	<	<	100.4	12	2.96	1.99	0.00	1.82	0.00	0.02	0.91	0.34	0.00	0.00	8.04		0.67	0.11	0.01
1612a Bt	37.04	17.31	2.32	13.45	0.10	<	16.00	<	0.37	8.96	95.6	11	2.73	1.50	0.13	0.83	0.01	0.00	1.75	0.00	0.05	0.84	7.84		0.32		
1612a Pl	62.86	23.77	<	0.07	<	<	<	5.20	8.74	0.13	100.8	8	2.76	1.23	0.00	0.00	0.00	0.00	0.00	0.25	0.75	0.01	5.00	0.25			

Mineral abbreviations after Kretz (1983).
The symbol '<' denotes below electron microprobe detection limit.
FeO* denotes that all Fe is treated as FeO.

Table 3. Electron microprobe analyses for garnet amphibolite samples.

	SiO_2	Al_2O_3	TiO_2	FeO*	Cr_2O_3	MnO	MgO	CaO	Na_2O	K_2O	Total	#O	Si	Al	Ti	Fe	Cr	Mn	Mg	Ca	Na	K	Total	X_{an}	Fe#	X_{grs}	X_{sps}
9730h2 Grt	37.02	21.30	0.12	27.79	0.06	1.89	2.19	9.96	<	<	100.3	12	2.95	2.00	0.01	1.85	0.00	0.13	0.26	0.85	0.00	0.00	8.05		0.877	0.28	0.041
9730h2 Am[a]	40.51	16.33	0.94	19.29	<	0.27	6.97	11.29	1.48	0.76	97.8	23	6.12	2.91	0.11	2.44	0.00	0.04	1.57	1.83	0.43	0.15	15.58		0.61		
9730h2 Pl	60.79	24.26	<	0.09	<	<	<	5.73	8.32	0.05	99.3	8	2.72	1.28	0.00	0.00	0.00	0.00	0.00	0.27	0.72	0.00	5.00	0.27			
9731d1 Grt	36.95	21.40	<	27.36	<	2.23	2.15	9.35	<	<	99.4	12	2.96	2.02	0.00	1.83	0.00	0.15	0.26	0.80	0.00	0.00	8.03		0.88	0.26	0.05
9731d1 Am[a]	39.56	18.62	0.66	17.84	<	0.15	6.57	11.56	1.27	0.98	97.2	23	5.98	3.32	0.08	2.26	0.00	0.02	1.48	1.87	0.37	0.19	15.56		0.60		
9731d1Pl	60.98	24.65	<	0.05	<	<	<	6.28	7.88	0.14	100.0	8	2.71	1.29	0.00	0.00	0.00	0.00	0.00	0.30	0.68	0.01	4.99	0.30			
9817g Grt	38.05	21.26	0.06	26.56	<	0.91	3.44	9.74	<	<	100.1	12	3.00	1.97	0.00	1.75	0.00	0.06	0.40	0.82	0.00	0.00	8.01		0.81	0.27	0.02
9817g Am[a]	41.55	15.15	0.89	17.08	0.36	0.24	8.32	11.75	1.15	0.95	97.4	23	6.24	2.68	0.10	2.15	0.04	0.03	1.86	1.89	0.34	0.18	15.52		0.54		
9817g Pl	56.32	28.09	<	0.10	<	<	<	10.08	5.76	0.05	100.4	8	2.52	1.48	0.00	0.00	0.00	0.00	0.00	0.48	0.50	0.00	4.99	0.49			
1623a Grt	37.24	21.31	0.05	28.08	<	0.92	5.49	6.83	<	<	100.0	12	2.94	1.98	0.00	1.85	0.00	0.06	0.65	0.58	0.00	0.00	8.07		0.74	0.18	0.02
1623a Am[a]	42.16	13.51	1.10	17.65	0.07	0.27	9.54	10.59	1.49	0.66	97.0	23	6.35	2.40	0.12	2.23	0.01	0.04	2.14	1.71	0.44	0.13	15.56		0.51		
1623a Pl	61.36	24.48	<	0.05	<	<	<	6.26	7.86	0.14	100.2	8	2.72	1.28	0.00	0.00	0.00	0.00	0.00	0.30	0.68	0.01	4.98	0.30			
9806f Grt	38.71	22.02	<	25.69	<	0.61	7.03	6.94	<	<	101.0	12	2.97	1.99	0.00	1.65	0.00	0.04	0.81	0.57	0.00	0.00	8.03		0.67	0.19	0.013
9806f Am[a]	43.87	11.85	1.19	13.94	<	0.17	12.18	11.49	1.24	0.61	96.5	23	6.52	2.08	0.13	1.73	0.00	0.02	2.70	1.83	0.36	0.12	15.47		0.39		
9806f Pl	56.71	27.37	<	0.36	<	<	<	9.36	6.01	0.05	99.9	8	2.55	1.45	0.00	0.01	0.00	0.00	0.00	0.45	0.52	0.00	4.99	0.46			
1617c Grt	39.22	21.98	0.06	26.11	0.07	0.62	7.66	5.65	<	<	101.4	12	2.99	1.98	0.00	1.67	0.00	0.04	0.87	0.46	0.00	0.00	8.02		0.66	0.15	0.013
1617c Am[a]	41.99	15.91	0.54	14.85	0.25	0.16	10.47	10.69	1.71	0.50	97.1	23	6.24	2.79	0.06	1.85	0.03	0.02	2.32	1.70	0.49	0.09	15.59		0.44		
1617c Pl	57.85	26.95	<	0.08	<	<	<	8.49	6.43	0.19	100.0	8	2.59	1.42	0.00	0.00	0.00	0.00	0.00	0.41	0.56	0.01	4.99	0.42			

Mineral abbreviations after Kretz (1983) and Bucher & Frey (1994).
The symbol '<' denotes below electron microprobe detection limit.
FeO* denotes that all Fe is treated as FeO.

Table 4. Electron microprobe analyses for eclogite samples.

	SiO_2	Al_2O_3	TiO_2	FeO*	Cr_2O_3	MnO	MgO	CaO	Na_2O	K_2O	Total	#O	Si	Al	Ti	Fe^a	Cr	Mn	Mg	Ca	Na	K	Total	Fe#	X_{grs}	X_{sps}
9801e5 Grt	38.51	21.91	<	24.69	<	0.16	6.11	8.79	<	<	100.2	12	2.98	2.00	0.00	1.60	0.00	0.01	0.70	0.73	0.00	0.00	8.02	0.69	0.24	0.003
9801e5 Cpx	54.82	6.90	0.08	5.79	<	<	10.05	18.71	2.88	<	99.3	6	2.00	0.30	0.00	0.18	0.00	0.00	0.55	0.73	0.20	0.00	3.95	0.24		
9803c Grt	37.39	21.54	<	25.25	<	0.63	3.08	11.38	<	<	99.3	12	2.97	2.01	0.00	1.67	0.00	0.04	0.36	0.97	0.00	0.00	8.02	0.82	0.32	0.01
9803c Cpx	52.81	1.49	<	11.01	<	0.09	11.92	21.86	0.77	<	100.0	6	1.99	0.07	0.00	0.35	0.00	0.00	0.67	0.88	0.06	0.00	4.01	0.34		
9803c Phe	49.21	28.21	0.62	2.68	<	<	3.04	<	0.08	11.68	95.6	11	3.31	2.24	0.03	0.15	0.00	0.00	0.30	0.00	0.01	1.00	7.04	0.33		
9804d Grt	39.26	22.49	<	22.68	<	0.42	8.11	7.68	<	<	100.7	12	2.98	2.01	0.00	1.44	0.00	0.03	0.92	0.63	0.00	0.00	8.01	0.61	0.21	0.009
9804d Cpx	54.79	9.33	<	5.05	<	0.19	9.19	17.98	2.51	0.05	99.1	6	1.98	0.40	0.00	0.15	0.00	0.01	0.50	0.70	0.18	0.00	3.91	0.24		
9819f Grt	37.97	21.34	<	27.32	<	0.30	5.03	8.10	<	<	100.1	12	2.98	1.97	0.00	1.79	0.00	0.02	0.59	0.68	0.00	0.00	8.03	0.75	0.22	0.007
9819f Cpx	53.24	4.23	0.05	9.58	<	0.09	11.09	19.16	2.25	<	99.7	6	1.98	0.19	0.00	0.30	0.00	0.00	0.62	0.76	0.16	0.00	4.01	0.33		
9808i3 Grt	38.88	22.16	<	22.29	<	0.27	6.57	10.38	<	<	100.6	12	2.98	2.00	0.00	1.43	0.00	0.02	0.75	0.85	0.00	0.00	8.02	0.66	0.28	0.006
9808i3 Cpx	53.98	4.41	0.09	6.91	<	0.08	11.56	20.68	1.49	<	99.2	6	1.99	0.19	0.00	0.21	0.00	0.00	0.64	0.82	0.11	0.00	3.96	0.25		
9808f1 Grt	38.73	22.06	0.04	24.39	<	0.49	6.31	8.52	<	<	100.5	12	2.98	2.00	0.00	1.57	0.00	0.03	0.72	0.70	0.00	0.00	8.02	0.68	0.23	0.011
9808f1 Cpx	57.01	12.42	0.04	3.98	0.12	0.05	7.56	15.31	4.65	0.15	101.3	6	1.99	0.51	0.00	0.12	0.00	0.00	0.39	0.57	0.32	0.01	3.91	0.23		
9809m Grt	38.57	22.03	0.09	25.51	<	0.63	6.85	6.81	<	<	100.5	12	2.97	2.00	0.01	1.65	0.00	0.04	0.79	0.56	0.00	0.00	8.02	0.68	0.19	0.014
9809m Omp	56.09	10.61	0.05	4.06	<	<	8.71	13.37	6.85	<	99.8	6	2.00	0.45	0.00	0.12	0.00	0.00	0.46	0.51	0.47	0.00	4.01	0.21		
9814i4 Grt	39.50	22.13	<	22.89	0.38	0.98	9.77	5.59	<	<	101.3	12	2.98	1.97	0.00	1.44	0.02	0.06	1.10	0.45	0.00	0.00	8.03	0.57	0.15	0.021
9814i4 Opx	54.39	0.04	0.05	18.12	0.06	0.30	26.06	0.30	<	<	99.7	6	1.99	0.02	0.00	0.55	0.00	0.01	1.42	0.01	0.00	0.00	4.00	0.28		
9813a Grt	39.21	22.84	<	18.39	<	0.35	11.26	8.06	<	<	100.1	12	2.94	2.02	0.00	1.15	0.00	0.02	1.26	0.65	0.00	0.00	8.05	0.48	0.21	0.007
9813a Omp	55.60	9.78	0.08	3.37	<	<	10.29	15.78	5.22	<	100.2	6	1.98	0.41	0.00	0.10	0.00	0.00	0.55	0.60	0.36	0.00	4.00	0.16		
9812a2 Grt	38.70	22.45	0.07	26.22	<	0.41	9.29	3.82	<	<	101.0	12	2.95	2.02	0.00	1.67	0.00	0.03	1.06	0.31	0.00	0.00	8.04	0.61	0.10	0.009
9812a2 Cpx	52.78	2.49	0.25	9.00	<	0.16	12.97	20.78	1.20	<	99.7	6	1.97	0.11	0.01	0.28	0.00	0.01	0.72	0.83	0.09	0.00	4.01	0.28		
9813e Grt	39.30	22.29	<	22.04	<	0.39	9.31	7.41	<	<	100.8	12	2.97	1.99	0.00	1.39	0.00	0.03	1.05	0.60	0.00	0.00	8.03	0.57	0.20	0.008
9813e Omp	56.09	11.53	0.13	4.36	<	<	8.11	12.69	7.22	<	100.2	6	1.99	0.48	0.00	0.13	0.00	0.00	0.43	0.48	0.50	0.00	4.01	0.23		

Mineral abbreviations after Kretz (1983) and Bucher & Frey (1994).
The symbol '<' denotes below electron microprobe detection limit.
FeO* denotes that all Fe is treated as FeO.
[a]$Fe^{3+}/Fe^{total} = 0.3$ for all samples, based on omphacite remaining in samples 9809m, 9813a, and 9813e.

Pressure and temperature estimates were made using the May 2001 thermodynamic dataset and THERMOCALC version 3.1 software of Powell & Holland (1988); error ellipses show ±1 standard deviation. Equilibration conditions for metapelite were determined from the intersections of the garnet–biotite (GARB) and garnet–aluminium-silicate–silica–plagioclase (GASP) or garnet–biotite–muscovite–plagioclase (GBMP) reactions, or from the intersection of reactions involving additional minerals, e.g. staurolite. Equilibration conditions for garnet amphibolite were determined from the intersection of the garnet–plagioclase–hornblende–quartz (GPHQ) and garnet–hornblende (GARHB) reactions. Assessing the pressures and temperatures of eclogite was more difficult, as it generally lacks phengite, kyanite, orthopyroxene, and albite. Minimum pressures were derived from the albite–jadeite–quartz barometer and temperatures were derived from the Krogh Ravna (2000) garnet–clinopyroxene thermometer. For sample 9803c, pressure and temperature were determined from the intersection of the Krogh Ravna (2000) garnet–clinopyroxene thermometer and the Waters & Martin (1993) garnet–clinopyroxene–phengite barometer. The sample of orthopyroxene-bearing eclogite (9814i4) was analysed using the garnet–orthopyroxene Fe–Mg exchange

thermometer of Carswell & Harley (1990) and the garnet–orthopyroxene barometer of Aranovich & Berman (1997).

Retrogression impeded the ability to recover mineral compositions established at peak pressures and temperatures. While most garnet, plagioclase and amphibole grains in the samples retain growth zoning, most biotite grains are homogeneous as a result of the rapid volume diffusion that is characteristic of biotite at amphibolite-facies conditions. This missing record of biotite–garnet prograde equilibration prohibits the retrieval of *P–T* conditions from the mineral cores in pelitic rocks. It is possible, however, to estimate a minimum peak temperature for the rocks by pairing the minimum Fe# [Fe/(Fe + Mg)] of garnet with the maximum Fe# of matrix biotite (Spear *et al.*, 1991). It was presumed that during cooling, garnet and biotite exchanged Fe and Mg such that the Fe# of garnet increased and the Fe# of biotite decreased at grain rims. Where retrograde net-transfer reactions consumed garnet, the excess Fe from the consumed garnet was added to the biotite, causing the Fe# of the biotite to increase at the rim rather than decrease. This retrograde garnet consumption also produced a 'well' in the Fe# profile of the garnet grain and a Mn spike near the grain rim. Following Kohn & Spear (2000), the effects of garnet consumption were removed by using the extra Mn forced back into the garnet grain during resorption as a measure of the volume of dissolved garnet. This method yields the pre-retrogression Fe# of biotite, which is then paired with the minimum Fe# of garnet to yield a corrected estimate of peak temperature. The amount of resorption experienced by garnet grains in this study varies greatly (from 5 to 1000 μm) but is generally $< 10\%$ of the grain diameter (Table 1). The exceptions include two partially homogenized grains of garnet (1622f1 and 9804j1), to which the Kohn & Spear (2000) method cannot be applied. Another exception, 9819d1, contains staurolite that grew at the expense of garnet and thus increased the amount of garnet resorption (Florence & Spear, 1993; Florence *et al.*, 1993). Garnet zoning established during prograde metamorphism may also be erased by volume diffusion at amphibolite-facies conditions; the γ' parameter of Lasaga (1983) was used to identify garnet grains with diffusionally modified core compositions.

Because Ca diffusion in plagioclase is slow (Spear & Daniel, 2001), matrix plagioclase grains distant from garnet are considered least affected by retrograde net-transfer reactions, and the rims of these grains are taken to reflect X_{an} at peak temperature conditions. This composition of the plagioclase rims was paired with the composition of garnet at the Fe# well to determine the pressure at the peak temperature. In most of the samples, garnet Ca zoning decreases rimward by 0.01–0.08 X_{grs} toward the Fe# well before decreasing further to the rim, demonstrating that the cores of the garnet grains record the highest apparent pressure. In samples 9816f, 1627c, and 9730g2, however, X_{grs} increases from the core to just before the Fe# well before falling at the rim. In sample 9816f, the highest X_{grs} occurs about 90 μm (or at 8% of the present size of the garnet grain) from the Fe# well of the garnet grain; in this case, an improved estimate of peak pressure was retrieved using the Fe# well of the garnet for thermometry and the peak X_{grs} of the garnet for barometry.

Garnet amphibolite frequently contains Ca-bearing phases other than plagioclase (e.g. calcite, epidote, or titanite), resulting in a more complex relationship among pressure, X_{grs} and X_{an}. For these samples, the pressure at peak temperature was determined from the net-transfer of Al and Ca between amphibole, plagioclase and garnet. Again, because Al diffuses slowly, the rims of matrix grains far from garnet were considered to be unaffected by retrograde net-transfer reactions, and these points were paired with the Fe# well compositions of garnet. For samples in which the Fe# of amphibole was homogeneous, peak temperature was calculated by matching the outermost, non-retrograde point of the amphibole with the composition of the garnet grain at the Fe# well. The method of Kohn & Spear (2000) cannot be used to remove the effects of retrogression in garnet amphibolite because of the complexity of the reactions between garnet and amphibole; therefore these estimates of peak temperature are minima.

Mineral compositions for thermobarometry of eclogite were chosen using the rationale of Carswell *et al.* (2000): peak temperature was calculated from the Fe# well of garnet, the maximum Fe# of omphacite, and, where applicable, the maximum Fe# of phengite; peak pressure was obtained using the maximum jadeite component in omphacite, the maximum $a_{prp}\ a_{grs}^2$ in garnet, and, where possible, the highest Si phengite. Omphacite is preserved in three samples (9809m, 9813e, and 9813a). For the rest of the samples, clinopyroxene + plagioclase symplectites were analysed, and jadeite activity was calculated using the scheme of Holland (1990).

The presence of orthopyroxene in sample 9814i4 provides a means of determining metamorphic pressure. In this rock, the lowest Fe# of garnet yields a minimum estimate of peak temperature when paired with the lowest Fe# of orthopyroxene, assuming that the increase in Fe# at the rim of the orthopyroxene is the result of retrograde net-transfer reactions.

P–T PATHS

Garnet chemical zoning was used to recover the *P–T* path followed by the rocks. For the pelitic rocks, the program GIBBS version 2.01 (Spear & Menard, 1989) was employed to contour the components and modes of different minerals in *P–T* space. The Gibbs method determines changes in pressure and temperature as a function of the change in mineral chemistry (modified by diffusion) by solving a series of linear differential equations to derive the slopes of *P*, *T* and *X* isopleths.

The variables of the system include the differentials of temperature, pressure and chemical potential, plus the individual compositional terms of the solid solutions (Spear & Selverstone, 1983). Because of partial garnet resorption, mineral components were contoured only for the core and peak temperature (garnet Fe# well) compositions of the garnet.

RESULTS

Allochthon garnet displays prograde zoning with bell-shaped Mn curves and rimward-decreasing Fe#; evidence of resorption appears as a reversal in zoning tens of micrometers from the grain rims (Fig. 5a). Garnet from samples 1622f1, 1622f2, and 9804j1 is the only allochthon garnet to have been partially homogenized (Mn is homogeneous but Fe, Mg, and Ca retain partial original zoning), while both basement metapelite samples have completely homogeneous garnet (Fig. 5b,c). The γ' parameter of Lasaga (1983) shows that garnet in sample 9816f most likely also experienced diffusional modification of the core, even though the garnet was not homogenized.

Metapelite samples across the entire study area yield uniform pressures of 10–12 kbar at peak temperature (Table 5, Fig. 6a). This is particularly surprising in light of the reported westward-increasing eclogite and granulite temperature gradient across the WGR (Griffin *et al.*, 1985). The peak temperatures recorded by basement garnet are similar to those of the allochthons (825 °C for 9804c1 and 713 °C for 9809o2), but the pressures are considerably lower: 7.0 and 6.2 kbar, respectively. Three samples (1605b, 9819d1, and 9817g2a) yield temperatures slightly below the stability

Table 5. Thermobarometry results.

Sample	Thermometer	Barometer	T (°C)	P (kbar)	Correlation coefficient
9730g2	GrtBtPlQtzKySt	Intersection	656 ± 116	9.7 ± 2.2	0.940
9730g3	GrtBtPlQtzKySt	Intersection	661 ± 110	9.7 ± 2.1	0.920
1605a	GrtBt	GrtKyAnQtz	658 ± 50	10.1 ± 1.0	0.600
1605b[a]	GrtBt	GrtKyAnQtz	655 ± 50	10.5 ± 1.0	0.600
9731I	GrtBt	GrtBtMsPl	665 ± 61	10.4 ± 1.1	0.889
9731d2	GrtBt	GrtBtMsPl	769 ± 72	11.5 ± 1.2	0.915
9817g2a[a]	GrtBt	GrtKyAnQtz	650 ± 50	10.5 ± 1.0	0.600
1627c	GrtBt	GrtBtMsPl	687 ± 63	9.7 ± 1.0	0.891
9816f	GrtBt	GrtKyAnQtz	615 ± 50	9.7 ± 1.0	0.600
9804c1[b]	GrtBt	GrtBtMsPl	825 ± 79	7.0 ± 1.0	0.814
9819d1[a]	GrtBtPlQtzMsKySt	Intersection	640 ± 68	11.5 ± 1.5	0.865
9804j1[b]	GrtBt	GrtBtMsPl	860 ± 76	10.8 ± 1.1	0.829
1622f1[b]	GrtBt	GrtKyAnQtz	836 ± 50	11.4 ± 1.0	0.600
1622f2[b]	GrtBt	GrtKyAnQtz	823 ± 50	12.5 ± 1.0	0.600
9809o2[b]	GrtBt	GrtBtMsPl	713 ± 71	6.2 ± 0.9	0.846
1612a	GrtBt	GrtKyAnQtz	710 ± 50	11.7 ± 1.0	0.600
9730h2	GrtHbl	GrtPlHblQtz	654 ± 49	10.3 ± 1.1	0.745
9731d1	GrtHbl	GrtPlHblQtz	625 ± 46	11.1 ± 1.0	0.814
9817g	GrtHbl	GrtPlHblQtz	682 ± 48	8.6 ± 0.9	0.670
1623a	GrtHbl	GrtPlHblQtz	794 ± 55	9.6 ± 1.7	0.501
9806f[b]	GrtHbl	GrtPlHblQtz	754 ± 51	8.9 ± 1.2	0.518
1617c	GrtHbl	GrtPlHblQtz	756 ± 51	9.5 ± 1.0	0.583
9801e5	GrtCpx	AbJdQtz	702 ± 50	18.4 (min)	
9803c	GrtCpx	GrtCpxPhe	691 ± 50	17.6 ± 1.0	0.600
9804d	GrtCpx	AbJdQtz	753 ± 50	16.7 (min)	
9819f	GrtCpx	AbJdQtz	664 ± 50	11.9 (min)	
9808i3	GrtCpx	AbJdQtz	779 ± 50	14.0 (min)	
9808f1[b]	GrtCpx	AbJdQtz	659 ± 50	14.1 (min)	
9814i4[b]	GrtOpx	GrtOpx	831 ± 50	28.5 ± 1.0	0.600
9809m	GrtCpx	AbJdQtz	486 ± 50	10.8 (min)	
9813a[b]	GrtCpx	AbJdQtz	760 ± 50	15.3 (min)	
9812a2[b]	GrtCpx	AbJdQtz	665 ± 50	7.9 (min)	
9813e[b]	GrtCpx	AbJdQtz	658 ± 50	14.4 (min)	

Mineral abbreviations after Kretz (1983) and Bucher & Frey (1994).
Correlation coefficient from THERMOCALC version 3.1 with May 2001 database (Powell & Holland, 1988).
'Intersection' is the intersection of the listed minerals from THERMOCALC.
(min) means minimum pressure estimate.
[a]Minimum PT estimates: thermobarometry estimates corrected for mineral assemblage.
[b]Samples contain partially to fully homogenized garnet.

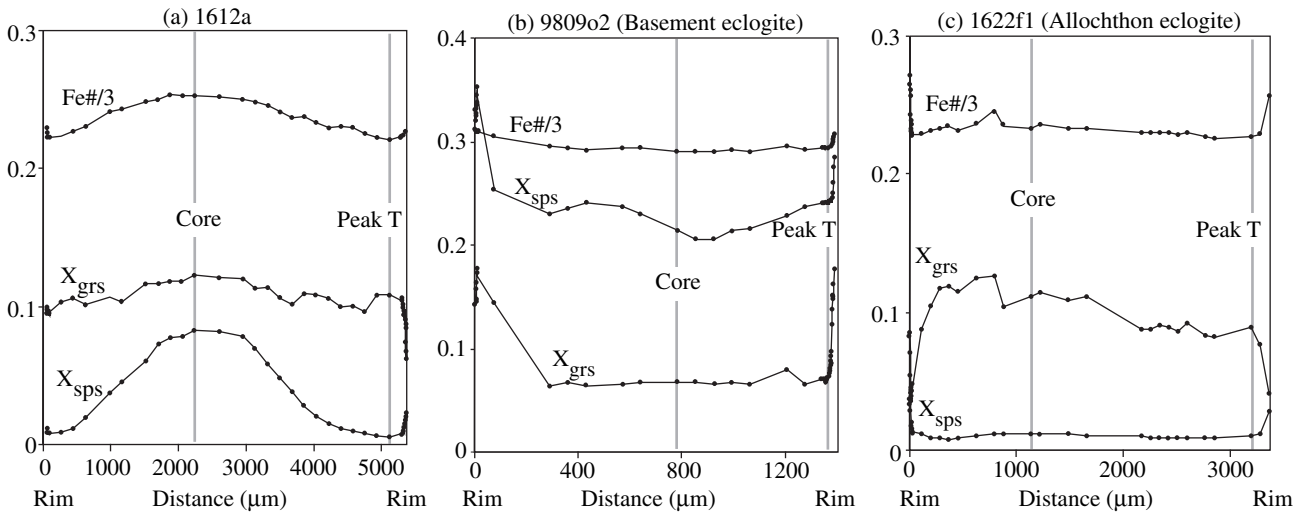

Fig. 5. (a) Representative metapelite prograde chemical zoning profiles – bell-shaped Mn and rimward decreasing Fe – shown for sample 1612a. Slightly decreasing X_{grs} indicates decreasing pressure (in the absence of other major Ca-bearing phases). At the very edge of the grain, a reversal in zoning indicates retrograde garnet resorption. The compositional points used for core and peak temperature thermobarometry are marked. (b, c) Chemical zoning profiles for representative garnet from samples 9809o2 and 1622f1. Flat or reversely zoned X_{sps} profiles show that the garnet has been at least partially homogenized. Note that while the Fe# increases at the rims of both garnet grains, the X_{grs} increases at the rim of basement sample 9809o2, suggesting compression, and decreases at the rim of allochthon sample 1622f1, suggesting decompression.

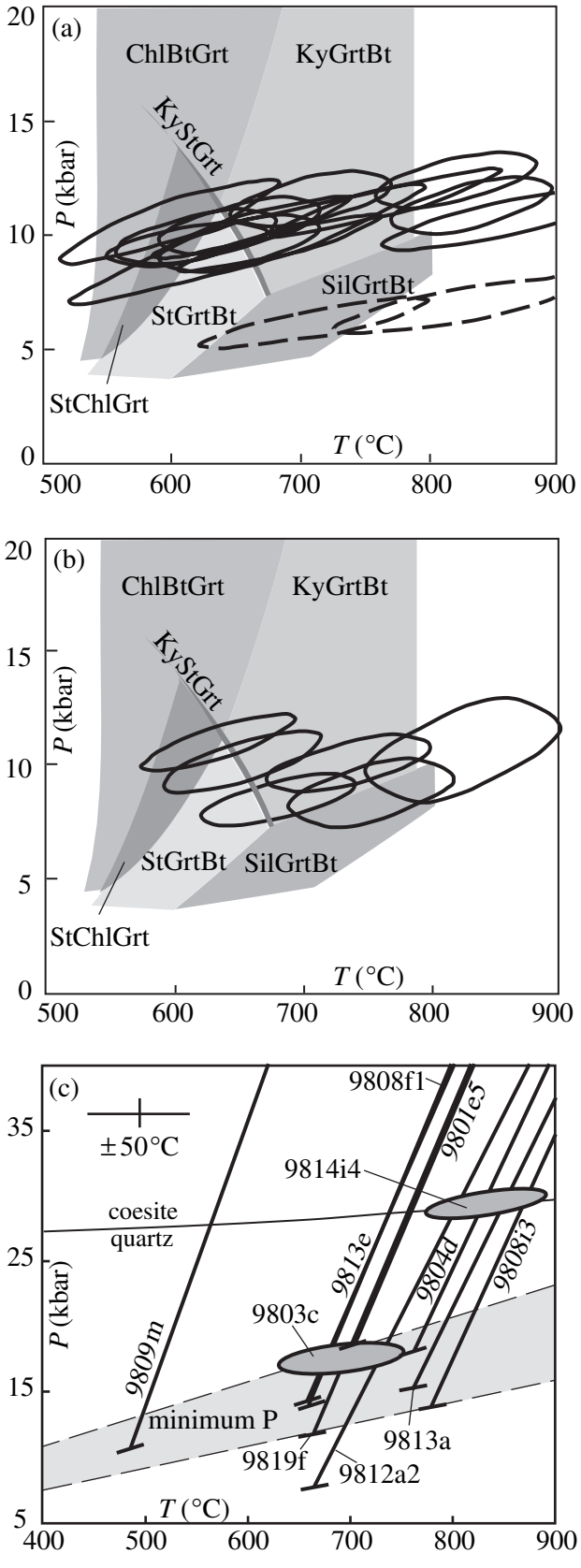

Fig. 6. (a) Peak temperature estimates for metapelite samples; error ellipses show ± 1 standard deviation. Dashed ellipses mark basement samples. The hottest samples contain partially homogenized garnet. Stability fields for certain mineral assemblages are shown in shades of grey, with mineral abbreviations after Kretz (1983). (b) Peak temperature estimates for garnet amphibolite samples, which yield pressures *c*. 1 kbar less than, but within error of, metapelite pressures at peak temperature. Hottest sample has partially homogenized garnet. (c) Peak temperature estimates for eclogite. Diagonal lines represent garnet–clinopyroxene Fe–Mg exchange reactions; the short diagonal lines at the base of each exchange reaction represent the minimum pressure for each sample determined from the albite = jadeite + quartz reaction. The shaded zone at the base represents the broad range of minimum pressures calculated for most of these samples. *P*–*T* determinations for phengite-bearing eclogite (9803c) and orthopyroxene-bearing eclogite (9814i4) are depicted as error ellipses.

field of their respective mineral assemblages, probably because of Fe–Mg exchange during retrogression; the temperatures for these samples were adjusted upward to agree with the mineral stability fields.

Geobarometry, Gibbs compositional contouring, and analysis of garnet zoning in most samples indicate a slight decrease in pressure from the core to the time of peak temperature growth. In more than half the garnet grains, this decompression is demonstrated by a continuous decrease from core to rim in X_{grs}, and is accompanied by an increase in X_{an} toward plagioclase rims. Garnet from five of the allochthon samples (9816f, 9731i, 9817g2a, 1627c, and 9730g2) records more complex X_{grs} profiles suggesting either compression with heating or isobaric heating from core to peak temperature followed by a plunge in X_{grs} at garnet rims. In distinct contrast to this, basement garnet shows X_{grs} profiles that are mostly flat, but have an increase in X_{grs} at the rim (Fig. 5b,c).

Garnet amphibolite across the study area records *P*–*T* estimates equivalent to those in the metapelite, emphasizing that all rocks in the allochthons across the WGR equilibrated at lower crustal pressures (Table 5, Fig. 6b). Calculated peak temperatures of garnet amphibolite are similar to peak temperatures in the metapelite, ranging from 625 ± 46 to 756 ± 51 °C, with one homogeneous garnet grain (from sample 1623a) yielding a higher temperature of 794 ± 55 °C. The pressures calculated at peak temperature for garnet amphibolite are approximately 1 kbar less than those of the metapelite, but are the same within uncertainty. Because these pressures are *c*. 50% higher than typical Barrovian metamorphism, this metamorphic overprint is referred to as 'supra-Barrovian'.

Peak temperatures calculated from eclogite are *c*. 650–780 °C (Table 5, Fig. 6c), with the exception of sample 9809m (486 ± 50 °C). There is no difference between peak temperatures calculated for basement eclogite and for the allochthon eclogite. Garnet in five of the samples in the northwestern portion of the field area was at least partially homogenized, while only two samples (9812a2 and 9813e) have completely

homogeneous garnet. All three samples retaining omphacite (9809m, 9813a, and 9813e) are located near metapelite containing homogeneous garnet.

One eclogite (9803c) containing phengite as inclusions within garnet yields a pressure estimate of 17.6 ± 1.0 kbar at peak temperature. The remaining calculated eclogite pressures, which are minima because of the lack of useful barometric assemblages, range from ≥7.9 to ≥18.4 kbar. Inclusions in garnet indicate prograde growth from epidote–amphibolite or amphibolite facies. The sample of orthopyroxene eclogite (9814i4) in the central part of the study area records a high peak temperature of 831 ± 50 °C, similar to metapelite temperatures in the area, and an ultrahigh pressure of 28.5 ± 1.0 kbar.

DISCUSSION

The identification of polycrystalline quartz pseudomorphs replacing coesite in sample 9809c3 expands the previously known UHP terrane of the WGR *c*. 50 km eastward. Unless this location proves to be an outlier surrounded only by HP rocks, this extension doubles the size of the UHP terrane in the Nordfjord–Stadlandet area from *c*. 1200 to 2300 km^2 and strongly alters the simple pressure gradient proposed by Cuthbert *et al*. (2000).

The spatial distribution of *P–T* estimates reveals that the allochthon pressures at peak temperature are identical across the entire study area. This consistency implies that the allochthons all equilibrated at lower crustal pressures (10–12 kbar) following the UHP metamorphism, and before being exhumed to the upper crust. Similar pressures reported for UHP and HP rocks exposed in the Nordøyane (Fig. 1; Terry *et al*., 2000; Terry & Robinson, 2003) and Sorøyane (Root, 2003) areas suggest that this supra-Barrovian metamorphism occurred across the entire WGR at a depth of *c*. 40 km. This may be an artifact of fluid availability during decompression (Proyer, 2003), but alternatively, the correspondence between this depth and the average thickness of continents (Christensen & Mooney, 1995) plus the decrease in exhumation rates at *c*. 35 km depth noted by Terry *et al*. (2000) and Carswell *et al*. (2003), suggest that the upward progress of the UHP rocks was arrested at the Moho. Figure 7 (Table 6) shows that even if the entire slab transformed to dense minerals (known to be untrue from Krabbendam *et al*., 2000; Wain *et al*., 2001) it was still significantly less dense than surrounding hydrous or anhydrous mantle lithosphere at both UHP and supra-Barrovian conditions; in contrast, at the Moho the former UHP slab was probably denser than average middle continental crust. If trapped at the Moho, the UHP terrane likely underwent large-scale buoyancy-driven flattening, supra-Barrovian metamorphism, and vertical collapse of the UHP to HP gradient that had developed in the slab. Analytical models of channel flow ignoring flexural rigidity (Bird, 1991) suggest that such a bolus of continental material at the Moho would flatten rapidly at these conditions (kinematic Moho wave of Fig. 8). At any reasonable strain rate, a 20-km thick UHP terrane would have been thinned to a few kilometres in 1–5 Myr. Simple Stoke's law calculations show that if viscosities in the range of 10^{16}–10^{19} Pa s (Kaufman & Royden, 1994; Clark & Royden, 2000) obtained for 1–5 Myr, eclogite and peridotite bodies differing in density from the gneiss by 0.5 kg m^{-3} and having radii of 10–100 m could have sunk several to several tens of kilometres

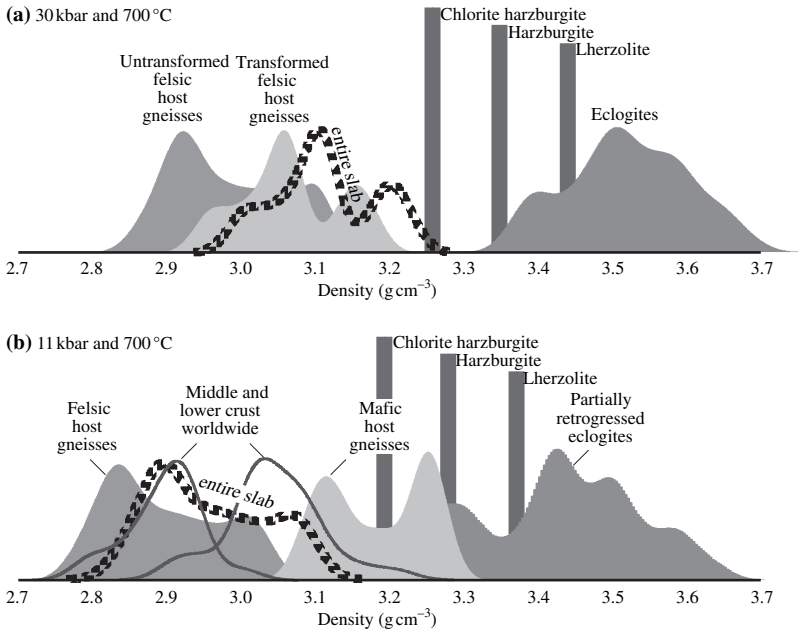

Fig. 7. Densities of rocks of the Western Gneiss Region at (a) UHP conditions (30 kbar and 700 °C) and (b) during the supra-Barrovian overprint at the Moho (11 kbar, 700 °C), calculated using the formalism of Hacker & Abers (2004) with an assumed uncertainty of ±0.03 g cm^{-3}. Mineral modes were obtained from Wain (1998) and by point counting thin sections from this study (Table 6); mineral compositions were taken from this study (Table 6) and Wain (1998). Lower and middle crustal densities were computed from V_P for lower and middle Palaeozoic orogens (Rudnick & Fountain, 1995) using the V_P–density relation of Christensen & Mooney (1995). To calculate the density of the bulk slab, 10 vol.% mafic rocks was assumed.

Table 6. Point-count data and calculated densities (this study).

Sample no.	9730g1	9730g2	9730g3	9730g4	9730h2	9730h3	9805a	1612a	9819d1
Rock type	Metapelite	Metapelite	Metapelite	Metapelite	Amphibolite	Amphibolite	Amphibolite	Metapelite	Metapelite
Bt	24.8	27.0	22.0	21.8	1.0	5.9	5.0	41.0	28.0
Chl		8.0	3.0	4.0					
Cpx									
Ep					3.0				
Grt	10.9	5.0	5.0	11.9	5.0	3.0	7.9	26.0	3.0
Am[b]	5.0			5.0	68.3	71.3	4.0		
Ilm	1.0			1.0	4.0	1.0		1.0	1.0
Kfs									
Ky							1.0	6.0	9.0
Ms	15.8	11.0	19.0	6.9					2.0
Pl	9.9	15.0	16.0	13.9	4.0	4.0	78.2	6.0	42.0
Qtz	32.7	32.0	34.0	35.6	11.9	11.9	1.0	20.0	15.0
Rt			1.0						
Ttn					3.0	3.0	3.0		
St		2.0							
Total	100	100	100	100	100	100	100	100	100
Density (g cm^{-3}) at 11 kbar and 700 °C	2.99	2.93	2.90	3.00	3.25	3.19	2.91	3.25	2.96
Density (g cm^{-3}) at 30 kbar and 700 °C	3.09	3.02	2.99	3.09	3.32	3.26	2.98	3.34	3.04

Sample no.	9731d1	9801f2	9813e	9813b1	9731n	9806e	9806h2	9731l1	9806f2	9810c1
Rock type	Retrogressed eclogite	Retrogressed eclogite	Eclogite	Eclogite	Mafic pod	Gabbro	Gabbro	Felsic gneiss	Felsic gneiss	Augen gneiss
Bt	5.0		11.0	2.0	16.8	10.0	9.8	16.2	17.0	22.0
Chl										
Cpx		29.0	44.0	55.4		10.0	4.9			
Ep										
Grt	25.0	42.0	41.0	17.8		11.0	10.8	7.1		
Am[b]	44.0	28.0		23.8	63.4	24.0	32.4		12.0	1.0
Ilm			2.0			2.0	3.9			1.0
Kfs										33.0
Ky										
Ms									1.0	
Pl	8.0	1.0			12.9	39.0	37.3	59.6	62.0	26.0
Qtz	18.0		2.0		6.9	4.0	1.0	17.2	8.0	16.0
Rt				1.0						
Ttn										1.0
St										
Total	100	100	100	100	100	100	100	100	100	100
Density (g cm^{-3}) at 11 kbar and 700 °C	3.25	3.54	3.55	3.43	3.09	3.11	3.14	2.87	2.84	2.78
Density (g cm^{-3}) at 30 kbar and 700 °C	3.32	3.60	3.61	3.48	3.17	3.18	3.20	2.95	2.92	2.86

Sample no.	9810m	9815c	9816a1	9809c	1613b	8822a11[a]	8825a3[a]	Y0815j2[a]	Y1611e[a]	Y0819a2[a]	Y0815f[a]
Rock type	HP augen gneiss	Felsic gneiss	Felsic gneiss	HP gneiss	Felsic gneiss	Felsic gneiss	Felsic gneiss	Biotite gneiss	Felsic gneiss	Felsic gneiss	Amphibolite gneiss
Bt	22.8	30.0	15.8		1.0	21.0	23.0	59.0	6.0	21.8	6.9
Chl											
Cpx	3.0			2.0							
Ep								12.0	8.0	13.9	11.9
Grt				38.8	12.0						25.7
Am[b]			5.0		17.0	9.0					5.9
Ilm				5.1			2.0				
Kfs							1.0				
Ky											
Ms				37.8			11.0		21.0	5.0	1.0
Pl	31.7	40.0	42.6		35.0	54.0	37.0	15.0	37.0	23.8	48.5
Qtz	41.6	30.0	36.6	16.3	35.0	16.0	26.0	12.0	28.0	35.6	
Rt											
Ttn	1.0							2.0			
St											
Total	100	100	100	100	100	100	100	100	100	100	100
Density (g cm^{-3}) at 11 kbar and 700 °C	2.83	2.82	2.80	3.35	2.96	2.84	2.84	3.02	2.81	2.88	3.03
Density (g cm^{-3}) at 30 kbar and 700 °C	2.92	2.91	2.89	3.42	3.04	2.92	2.93	3.11	2.90	2.97	3.10

Mineral abbreviations after Kretz (1983) and Bucher & Frey (1994).

The chosen samples are representative of the overall proportions of rock type across the study area. Densities were calculated from the point-count data above using the macro of Hacker & Abers (2004). Garnet, plagioclase, biotite and clinopyroxene mineral compositions were determined from electron microprobe analyses: metapelites: an30, grs15alm60prp25, ann50; amphibolites: an40, grs25alm55prp20; eclogites: grs20alm48prp32, jd50di25hd25.

HP and UHP mineral modes were recalculated assuming that the following reactions went to completion at HP and UHP: Ab = Jd + Qtz, An = Grs + Ky + Qtz, Hbl + Pl = Cpx, Qtz = Cs, Bt + Pl = Phe.

[a]Samples from D. Root and D. Young (pers. comm.). [b]Undifferentiated amphibole.

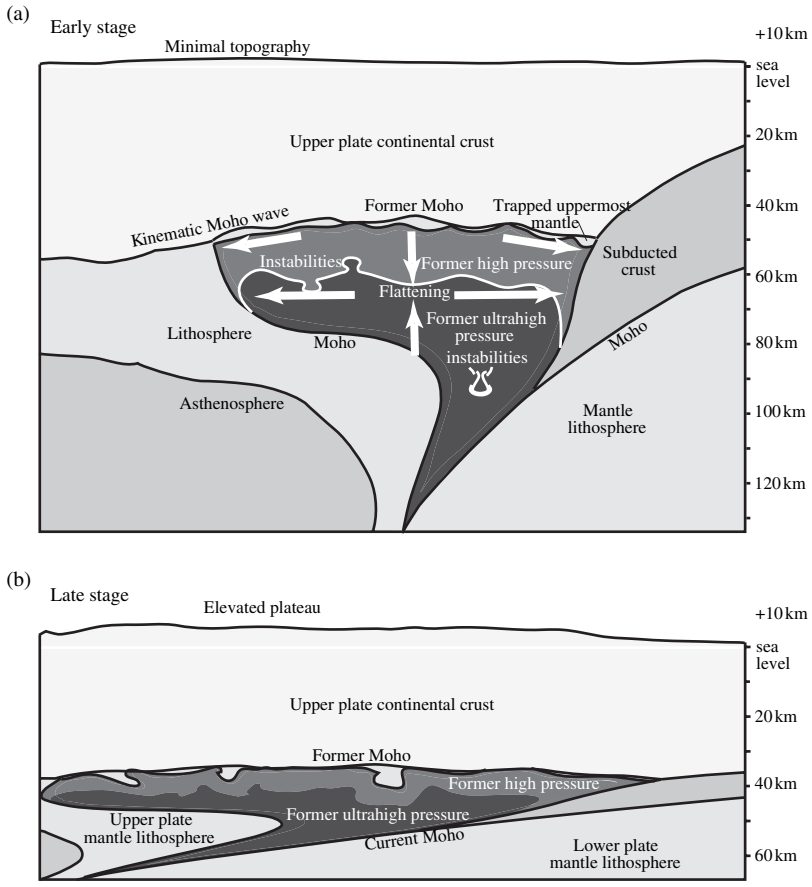

Fig. 8. (a, b) The exhuming UHP slab loses its positive buoyancy at the Moho. There it undergoes large-scale, buoyancy-driven flattening causing a wave-like disturbance of the Moho; supra-Barrovian metamorphism; collapse of the UHP (black) to HP (dark grey) gradient that had developed in the slab, and internal buoyancy-driven mixing and separation of rocks of different densities and, possibly, peak pressures. Some of the uppermost mantle may be trapped between the exhumed slab and the upper plate continental crust, resulting in the inclusion of peridotite bodies within the UHP/HP terrane. The sudden increase in crustal thickness – as well as probable change in elevation – may have driven subsequent crustal extension.

within the host gneiss (cf. Brueckner, 1998), potentially mixing rocks of different eclogite-facies pressures (Fig. 8); this could explain the large variations in pressure among nearby eclogite bodies noted by Wain *et al.* (2000).

Without an additional exhumation mechanism to raise them to Earth's surface, buoyancy considerations dictate that these UHP rocks should have remained at lower to middle crustal depths forever. Late Barrovian overprints are known from other well-exposed, well-studied UHP continental-subduction orogens [*c.* 475–550 °C, 5–8 kbar in the Dabie UHP–HP terrane (Hacker *et al.*, 1996; Liou *et al.*, 1996) and 625–675 °C, 8–10 kbar in the Kokchetav massif (Zhang *et al.*, 1997; Ota *et al.*, 2000)], suggesting that UHP rocks may commonly be arrested at the lower crust during exhumation. In light of this, it is possible that UHP rocks make up a significant portion of the middle to lower crust worldwide.

The UHP rocks of the WGR did not remain forever at the Moho, but were in fact exhumed before the UHP record could be erased. This second stage of exhumation – from the Moho to mid-upper crustal depths – is attributed mainly to top-W extension on orogen-scale shear zones such as the Nordfjord–Sogn Detachment (Fig. 1) (Andersen, 1998). The driving force for this exhumation is unknown but could have been influenced by the marked change in crustal thickness – and probable matching change in surface elevation (Fig. 8) – caused by the arrival of the UHP bolus at the Moho. The present crustal thickness of the WGR was probably extensively reworked during this extension, similar to the Basin and Range province of western North America (Klemperer *et al.*, 1986).

Considering the extent of the supra-Barrovian overprint in the allochthons, how was the eclogite preserved within such a pervasively recrystallized host gneiss? First, while there is evidence for older eclogite-facies metamorphic events within the Caledonides (see summary in Brueckner & van Roermund, 2004), U–Pb geochronology of zircon from eclogite across this study area shows that the eclogite was extensively affected by the Scandian metamorphism associated with the UHP event (Walsh *et al.*, unpubl. data). Hence, the eclogite was directly involved in the UHP and supra-Barrovian events. Second, barometry and Gibbs compositional contouring show that most of the allochthon metapelite underwent decompression to reach supra-Barrovian peak temperature conditions. The magnitude of decompression is hard to quantify because the compositions of minerals in equilibrium with garnet cores cannot be unambiguously determined – e.g. early biotite compositions were erased by volume diffusion. Also, nearly all decompression paths

within the garnet + kyanite + biotite stability field should have led to garnet consumption, and yet garnet does not exhibit evidence of the complex zoning that might be expected from prograde metamorphism, decompression, and then a supra-Barrovian overprint. Three possibilities are presented: (1) The eclogite formed *in situ*, and the peak-pressure garnet in the host rocks was (extensively) resorbed during decompression and then (almost) wholly reconstituted during the supra-Barrovian metamorphic overprint; (2) The eclogite, with the exception of the 28-kbar orthopyroxene eclogite and the eclogite with a quartz pseudomorph after coesite, formed *in situ* and only reached peak pressures of *c*. 18 kbar; (3) All the eclogite is exotic. Although Wain (1997) proved that the UHP eclogite west of the study area was metamorphosed *in situ*, the same cannot yet be proven for this study area. The eclogite is never bounded by obvious shear zones and is found in all rock types – metapelite, amphibolite, and gneiss – but because any mixing of eclogite and lower pressure rocks must have predated the supra-Barrovian overprint, evidence of the mixing could have been erased. Possibility (2) is essentially a variant of this, in which only the ultrahigh-pressure rocks would be exotic. Possibility (1), wholesale garnet resorption during decompression, seems equally viable and could be tested through geochronology of garnet cores.

There is a distinct difference in pressure of *c*. 4–5 kbar between the allochthon metapelite samples and the two basement metapelite samples. Moreover, while the bulk of the allochthon garnet shows a rimward loss of X_{grs} indicative of decompression, the basement garnet is homogeneous except for an increase in X_{grs} at grain rims that suggests compression (Fig. 5b,c). Again, the magnitude of compression is hard to quantify, due both to the effects of volume diffusion in biotite and to garnet resorption: thermobarometry of basement garnet rims yields >100 °C of isobaric cooling (Fig. 9) rather than compression. Geochronology is required to assess whether the high-temperature metamorphism was synchronous in the two units.

If the high-temperature metamorphism of the basement and allochthons *was* synchronous, the units occupied distinct structural levels (4–5 kbar apart) during metamorphism and were later juxtaposed by the thrusting of the higher pressure allochthons over the basement. If the high-temperature metamorphism occurred first in the basement, the allochthons must have been metamorphosed prior to being emplaced on top of the basement. There are no recognized shear zones or faults between the allochthons and the basement that might support either of these two possibilities, but the metamorphic temperatures are high enough that evidence of the juxtaposition could have been erased by annealing. If the high-temperature metamorphism occurred first in the allochthons, metamorphism of the basement could have happened

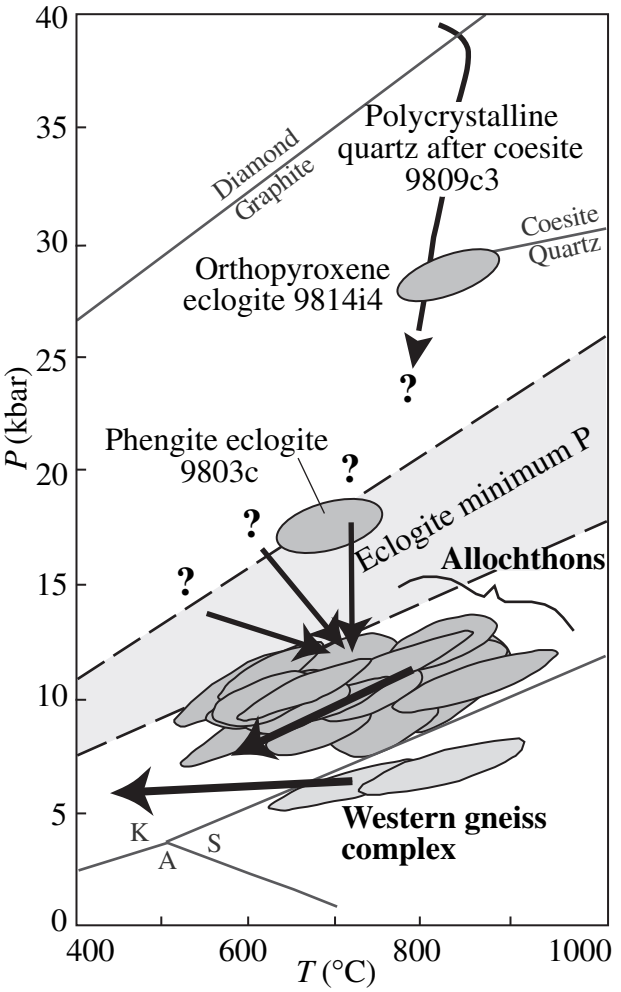

Fig. 9. Summary *P–T* diagram for the study area; bold arrows depict the inferred pressure–temperature path of the ultrahigh-pressure–high-pressure terrane. Ultrahigh pressures recorded by two eclogite samples were succeeded by 'supra Barrovian' metamorphism. The allochthon samples generally record heating and decompression to peak temperature followed by further decompression and cooling. Question marks show segments of the pressure–temperature path obliterated by retrogression. Basement garnet is homogeneous but records isobaric cooling at its rims. The allochthon and basement rocks were likely juxtaposed during cooling following the 'supra Barrovian' metamorphism. A = andalusite, K = kyanite, and S = sillimanite.

slightly later during continued and coupled exhumation of both units; this scenario seems the most likely.

Two tectonic scenarios (Fig. 10) that might have produced the metamorphic histories of the basement and allochthons in the study area are envisioned. (1) Exhumation was sufficiently slow that the slab passed (from east to west) progressively through Moho depths over a long time interval, and conductive and radiogenic heating caused each part of the slab to reach peak temperature as it passed through Moho depths. (2) The entire slab ascended quickly to the Moho, where it ponded at that neutrally buoyant level and

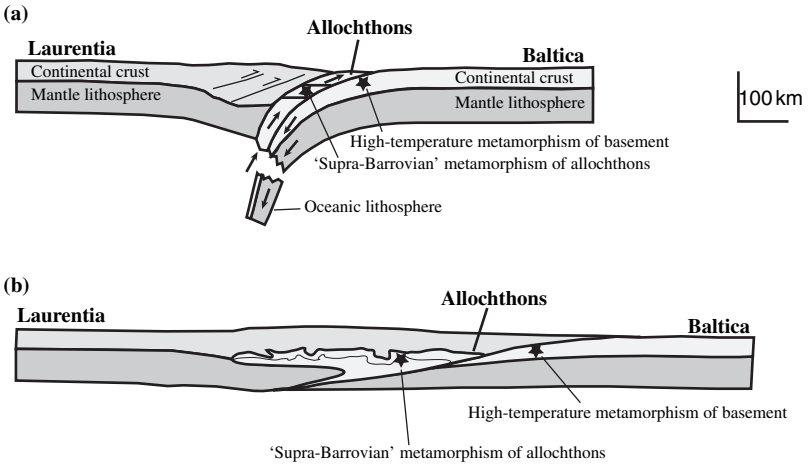

Fig. 10. Two tectonic scenarios that could have produced the observed *P–T* signatures of the allochthons and basement in the study area. (a) Exhuming allochthons rise progressively through Moho depths (after delamination from the mantle lithosphere). Conduction and radiogenic heating cause each portion of the allochthonous slab to reach peak temperatures while passing through 35–40 km depth. The basement undergoes peak temperature metamorphism at 20–25 km depth; the allochthons are thrust over the basement after 'supra Barrovian' metamorphism. (b) Ponding of the exhumed allochthons at the Moho. The basement undergoes peak temperature metamorphism at 20–25 km, and the allochthons are thrust over the basement after the 'supra Barrovian' metamorphism.

was subjected synchronously to lower crustal metamorphism. The widespread resetting of radiogenic Pb in titanite, zircon and monazite across the WGR at *c.* 395 Ma (Tucker *et al.*, 1987, 1990) suggests that the supra-Barrovian metamorphism was indeed synchronous across the slab, favouring scenario (2).

CONCLUSIONS

Thermobarometric results are interpreted to indicate that at least a 22 000 km^2 portion of the WGR UHP/HP terrane stalled at the Moho following exhumation through the mantle. At the Moho, the UHP/HP terrane underwent pronounced amphibolite-facies recrystallization and may have undergone concomitant large-scale buoyancy-driven flattening, vertical collapse of the UHP to HP gradient, and mixing of bodies of different densities. The UHP rocks were subsequently exhumed to mid-upper crustal levels, perhaps related to the crustal thickening caused by the arrest of the UHP/HP terrane at the Moho. Without this second stage of extension, the UHP/HP terrane could have remained in the lower crust. Such unexhumed UHP rocks may constitute a fundamental part of the lower to middle crust of orogens worldwide.

ACKNOWLEDGEMENTS

Helpful suggestions were gladly received from reviewers G. Franz, M. Terry, and H. Brueckner. This research was funded by National Science Foundation grant EAR-9814889, Sigma Xi, and the Geological Society of America. A special thanks to M. Krabbendam and D. Waters for helping us to obtain data from A. Wain's dissertation, to D. Root and D. Young for stimulating conversation in the field and lab, and to T. Onasch for his enthusiasm and support.

REFERENCES

Ajebli, M., 1995. Les gabbros coronitiques, partiellement éclogitisés, de Lom et de Lesja, Norvège. Doctorate Thesis, Université Paris 7-Denis Diderot University, France.

Andersen, T. B., 1998. Extensional tectonics in the Caledonides of southern Norway, an overview. *Tectonophysics*, **285,** 333–351.

Aranovich, L. Y. & Berman, R. G., 1997. A new garnet–orthopyroxene thermometer based on reversed Al_2O_3 solubility in FeO–Al_2O_3–SiO_2 pyroxene. *American Mineralogist*, **82,** 345–353.

Bird, P., 1991. Lateral extrusion of lower crust from under high topography, in the isostatic limit. *Journal of Geophysical Research*, **96,** 10275–10286.

Brueckner, H. K., 1977. A structural, stratigraphic and petrologic study of anorthosites, eclogites, and ultramafic rocks and their country rocks, Tafjord area, western south Norway. *Norges Geologiske Undersøkelse Bulletin*, **332,** 1–53.

Brueckner, H. K., 1998. Sinking intrusion model for the emplacement of garnet-bearing peridotites into continent collision orogens. *Geology*, **26,** 631–634.

Brueckner, H. K. & van Roermund, H. L. M., 2004. Dunk tectonics: A multiple subduction/eduction model for the evolution of the Scandinavian Caledonides. *Tectonics*, **23,** TC2004. doi: 10.1029/2003TC001502.

Bryhni, I. & Sturt, B. A., 1985. Caledonides of southwestern Norway. In: *The Caledonide Orogen–Scandinavia and Related Areas* (eds Gee, D. G. & Sturt, B. A.), pp. 89–108, John Wiley & Sons, Chichester, UK.

Bucher, K. & Frey, M., 1994. *Petrogenesis of Metamorphic Rocks*. Springer-Verlag, Berlin, Germany.

Carswell, D. A. & Harley, S. L., 1990. Mineral barometry and thermometry. In: *Eclogite Facies Rocks Reader in Metamorphic Petrology* (ed. Carswell, D. A.), pp. 396, Blackie and Son Ltd., Glasgow, UK.

Carswell, D. A., Harvey, M. A. & Al-Samman, A., 1983. The petrogenesis of contrasting Fe–Ti and Mg–Cr garnet

peridotite types in the high grade gneiss complex of Western Norway. *Bulletin de Mineralogie*, **106,** 727–750.
Carswell, D. A., Krogh, E. J. & Griffin, W. L., 1985. Norwegian orthopyroxene eclogites: calculated equilibration conditions and petrogenetic implications. In: *The Caledonide Orogen: Scandinavia and Related Areas*, pp. 823–841, John Wiley & Sons, Chichester, UK.
Carswell, D. A., Wilson, R. N. & Zhai, M., 2000. Metamorphic evolution, mineral chemistry and thermobarometry of schists and orthogneisses hosting ultra-high pressure eclogites in the Dabieshan of central China. *Lithos*, **52,** 121–155.
Carswell, D. A., Brueckner, H. K., Cuthbert, S. J., Mehta, K. & O'Brien, P. J., 2003. The timing of stabilisation and the exhermation rate for ultra-high pressure rocks in the Western Gneiss Region of Norway. *Journal of Metamorphic Geology*, **21,** 601–612.
Christensen, N. I. & Mooney, W. D., 1995. Seismic velocity structure and composition of the continental crust: a global view. *Journal of Geophysical Research*, **100,** 9761–9788.
Clark, M. K. & Royden, L. H., 2000. Topographic ooze: building the eastern margin of Tibet by lower crustal flow. *Geology*, **28,** 703–706.
Corfu, F., 1980. U–Pb and Rb–Sr systematics in a polyorogenic segment of the Precambrian shield, central southern Norway. *Lithos*, **13,** 305–323.
Cuthbert, S. J., Carswell, D. A., Krogh–Ravna, E. J. & Wain, A., 2000. Eclogites and eclogites in the Western Gneiss Region, Norwegian Caledonides. *Lithos*, **52,** 165–195.
Florence, F. P. & Spear, F. S., 1993. Influences of reaction history and chemical diffusion on *P–T* calculations for staurolite schists from the Littleton Formation, northwestern New Hampshire. *American Mineralogist*, **78,** 345–359.
Florence, F. P., Spear, F. S. & Kohn, M. J., 1993. *P–T* paths from Northwestern New Hampshire: metamorphic evidence for stacking in a thrust/nappe complex. *American Journal of Science*, **293,** 939–979.
Gee, D. G., 1975. A tectonic model for the central part of the Scandinavian Caledonides. *American Journal of Science*, **275A,** 468–515.
Gee, D. G. & Zachrisson, E., 1979. The Caledonides in Sweden. *Sveriges Geologiska Undersökning, Serie C, Avhandlingar och Uppsatser*, **73,** 48 pp.
Gee, D. G., Guezou, J.-C., Roberts, D. & Wolff, F. C., 1985. The central-southern part of the Scandinavian Caledonides. In: *The Caledonide Orogen – Scandinavia and Related Areas* (eds Gee, D. G. & Sturt, B. A.), pp. 109–133, John Wiley & Sons Ltd, Chichester, UK.
Griffin, W. L., Austrheim, H., Brastad, K. *et al*., 1985. High-pressure metamorphism in the Scandinavian Caledonides. In: *The Caledonide Orogen – Scandinavia and Related Areas* (eds Gee, D. G. & Sturt, B. A.), pp. 783–801, John Wiley & Sons, Chichester.
Guezou, J.-C., 1978. Geology and structure of the Dombås-Lesja area, southern Trondheim region, south-central Norway. *Norges Geologiske Undersøkelse*, **340,** 1–34.
Hacker, B. R. & Abers, G. A., 2004. Subduction Factory 3. An Excel worksheet and macro for calculating the densities, seismic wave speeds, and H_2O contents of minerals and rocks at pressure and temperature. *Geochemistry, Geophysics, and Geosystems*, **5,** DOI: 10.1029/2003GC000614.
Hacker, B. R. & Gans, P. B., in press. Continental collisions and the creation of ultrahigh-pressure terranes: The Trondelag–Jämtland region of the Scandinavian Caledonides. *Geological Society of America Bulletin*.
Hacker, B. R. & Peacock, S. M., 1995. Creation, preservation and exhumation of UHPM rocks. In: *Ultrahigh Pressure Metamorphism* (eds Coleman, R. G. & Wang, X.), pp. 159–181, Cambridge University Press, Cambridge, UK.
Hacker, B. R., Wang, X., Eide, E. A. & Ratschbacher, L., 1996. The Qinling–Dabie ultra-high-pressure collisional orogen. In: *The Tectonic Evolution of Asia* (eds Yin, A. & Harrison, T. M.), pp. 345–370, Cambridge University Press, Cambridge, UK.
Holland, T. J. B., 1990. Activities of components in omphacitic solid solutions: an application of Landau theory to mixtures. *Contributions to Mineralogy and Petrology*, **105,** 446–453.
Kaufman, P. S. & Royden, L. H., 1994. Lower crustal flow in an extensional setting: Constraints from the Halloran Hills region, eastern Mojave Desert, California. *Journal of Geophysical Research*, **99,** 15723–15739.
Klemperer, S. L., Hauge, T. A., Hauser, E. C., Oliver, J. E. & Potter, J. C., 1986. The Moho in the northern Basin and Range province, Nevada, along the COCORP 40°N seismic-reflection transect. *Geological Society of America Bulletin*, **97,** 603–618.
Kohn, M. J. & Spear, F. S., 2000. Retrograde net transfer reaction insurance for pressure–temperature estimates. *Geology*, **28,** 1127–1130.
Kollung, S., 1984. The Surnadal syncline revisited. *Norsk Geologisk Tidsskrift*, **64,** 257–262.
Kollung, S., 1990. The Surna, Rinna and Orkla Nappes of the Surnadal–Orkdal district, southwestern Trondheim Region. *Norges Geologiske Undersøkelse Bulletin*, **418,** 9–17.
Krabbendam, M., Wain, A. & Andersen, T. B., 2000. Pre-Caledonian granulite and gabbro enclaves in the Western Gneiss Region, Norway: indications of incomplete transition at high pressure. *Geological Magazine*, **137,** 235–255.
Kretz, R., 1983. Symbols for rock-forming minerals. *American Mineralogist*, **68,** 277–279.
Krill, A. G., 1985. Relationships between the Western Gneiss region and the Trondheim region: stockwerk tectonics reconsidered. In: *The Caledonide Orogen: Scandinavia and Related Areas* (ed. Gee, D. G.), pp. 475–483, John Wiley & Sons, Chichester, UK.
Krogh Ravna, E., 2000. The garnet–clinopyroxene Fe^{2+}–Mg geothermometer: an updated calibration. *Journal of Metamorphic Geology*, **18,** 211–219.
Lasaga, A. C., 1983. Geospeedometry: an extension of geothermometry. In: *Kinetics and Equilibrium in Mineral Reactions* (ed. Saxena, S. K.), pp. 81–114, Springer-Verlag, New York, NY, USA.
Liou, J. G., Zhang, R. Y., Eide, E. A., Maruyama, S., Wang, X. & Ernst, W. G., 1996. Metamorphism and tectonics of high-P and ultrahigh-P belts in Dabie-Sulu Regions, eastern central China. In: *The Tectonic Evolution of Asia* (eds Yin, A. & Harrison, T. M.), pp. 300–343, Cambridge University Press, Cambridge, UK.
Lutro, O., Robinson, P. & Solli, A., 1997. *Proterozoic Geology and Scandian High-Pressure Overprinting in the Western Gneiss Region, Norges*. Geologiske Undersøkelse, Trondheim, Norway.
Medaris, L. G., 1984. A geothermobarometric investigation of garnet peridotites in the Western Gneiss Region of Norway. *Contributions to Mineralogy and Petrology*, **87,** 72–86.
Milnes, A. G., Wennberg, O. P., Skår, Ø. & Koestler, A. G., 1997. Contraction, extension and timing in the South Norwegian Caledonides: the Sognefjord transect. In: *Orogeny Through Time* (eds Burg, J.-P. & Ford, M.), pp. 123–148, Geological Society Special Publications, The Geological Society, London, UK.
Ota, T., Terabayashi, M., Parkinson, C. D. & Masago, H., 2000. Thermobaric structure of the Kokchetav ultrahigh-pressure–high-pressure massif deduced from a north–south transect in the Kulet and Saldat–Kol regions, northern Kazakhstan. *The Island Arc*, **9,** 328–357.
Powell, R. & Holland, T. J. B., 1988. An internally consistent dataset with uncertainties and correlations: 3. Applications to geobarometry, worked examples and a computer program. *Journal of Metamorphic Geology*, **6,** 173–204.
Proyer, A., 2003. The preservation of high-pressure rocks during exhumation: metagranites and metapelites. *Lithos*, **70,** 183–194.
Roberts, D. & Gee, D. G., 1985. An introduction to the structure of the Scandinavian Caledonides. In: *The Caledonide Orogen – Scandinavia and Related Areas* (eds Gee, D. G. & Sturt, B. A.), pp. 55–68, John Wiley and Sons, Chichester, UK.

Robinson, P., 1995. Extension of Trollheimen tectono-stratigraphic sequence in deep synclines near Molde and Brattvåg, Western Gneiss Region, southern Norway. *Norsk Geologisk Tidsskrift*, **75,** 181–198.

van Roermund, H. L. M., Drury, M. R., Barnhoorn, A. & de Ronde, A., 2001. Relict majoritic garnet microstructures from ultra-deep orogenic peridotites in western Norway. *Journal of Petrology*, **42,** 117–130.

Root, D. B., 2003. Zircon geochronology of ultrahigh-pressure eclogites and exhumation of the Western Gneiss Region, southern Norway. Ph.D. Thesis. University of California, Santa Barbara, CA, USA.

Root, D. B., Hacker, B. R., Mattinson, J. M. & Wooden, J. L., in press. Zircon geochronology and ca. 400 Ma exhumation of Norwegian ultrahigh-pressure rocks: an ion microprobe and chemical abrasion study. *Earth and Planetary Science Letters*.

Root, D. B., Hacker, B. R., Gans, P., Eide, E., Ducea, M. & Mosenfelder, J., in review. Discrete ultrahigh-pressure domains in the Western Gneiss Region, Norway: implications for formation and exhumation. *Journal of Metamorphic Geology*.

Rudnick, R. L. & Fountain, D. M., 1995. Nature and composition of the continental crust: a lower crustal perspective. *Reviews of Geophysics*, **33,** 267–309.

Schärer, U., 1980. U–Pb and Rb–Sr dating of a polymetamorphic nappe terrain: the Caledonian Jotun Nappe, southern Norway. *Earth and Planetary Science Letters*, **49,** 205–218.

Spear, F. S. & Daniel, C. G., 2001. Diffusion control of garnet growth, Harpswell Neck, Maine, USA. *Journal of Metamorphic Geology*, **19,** 179–195.

Spear, F. S. & Menard, T., 1989. Program GIBBS: a generalized Gibbs. *American Mineralogist*, **74,** 942–943.

Spear, F. S. & Selverstone, J., 1983. Quantitative *P–T* paths from zoned minerals: theory and tectonic applications. *Contributions to Mineralogy and Petrology*, **83,** 348–357.

Spear, F. S., Kohn, M. J., Florence, F. P. & Menard, T., 1991. A model for garnet and plagioclase growth in pelitic schists: implications for thermobarometry and *P–T* path determinations. *Journal of Metamorphic Geology*, **8,** 683–696.

Strand, T., 1969. Geology of the Grotli area. *Norsk Geologisk Tidsskrift*, **49,** 341–360.

Svenningsen, O. M., 2001. Onset of seafloor spreading in the Iapetus Ocean at 608 Ma: precise age of the Sarek Dyke Swarm, northern Swedish Caledonides. *Precambrian Research*, **110,** 241–254.

Terry, M. P. & Robinson, P., 2003. Evolution of amphibolite-facies structural features and boundary conditions for deformation during exhumation of high- and ultrahigh-pressure rocks, Nordøyane, Western Gneiss Region, Norway. *Tectonics*, **22,** 1036. doi:10.1029/2001TC001349.

Terry, M. P., Robinson, P. & Krogh Ravna, E. J., 2000. Kyanite eclogite thermobarometry and evidence for thrusting of UHP over HP metamorphic rocks, Nordøyane, Western Gneiss Region, Norway. *American Mineralogist*, **85,** 1637–1650.

Torsvik, T. H., 1998. Palaeozoic palaeogeography: a North Atlantic viewpoint. *Geologiska Föreningens i Stockholm Förhandlingar*, **120,** 109–118.

Tucker, R. D., Råheim, A., Krogh, T. E. & Corfu, F., 1987. Uranium-lead zircon and titanite ages from the northern portion of the Western Gneiss Region, south-central Norway. *Earth and Planetary Science Letters*, **81,** 203–211.

Tucker, R. D., Krogh, T. E. & Råheim, A., 1990. Proterozoic evolution and age-province boundaries in the central part of the Western Gneiss region, Norway: results of U–Pb dating of accessory minerals from Trondheimsfjord to Geiranger In: *Mid-Proterozoic Laurentia-Baltica, GAC Special Paper* (eds Gower, C. F., Rivers, T. & Ryan, B.), pp. 149–173, Geological Association of Canada, St. John's, Newfoundland, Canada.

Wain, A., 1997. New evidence for coesite in eclogite and gneisses: Defining an ultrahigh-pressure province in the Western Gneiss region of Norway. *Geology*, **25,** 927–930.

Wain, A. L., 1998. Ultrahigh-Pressure Metamorphism in the Western Gneiss Region of Norway. Ph.D. Thesis, Oxford University, Oxford, UK.

Wain, A., Waters, D., Jephcoat, A. & Olijnyk, H., 2000. The high-pressure to ultrahigh-pressure transition in the Western Gneiss Region, Norway. *European Journal of Mineralogy*, **12,** 667–687.

Wain, A., Waters, D. J. & Austrheim, H., 2001. Metastability of granulites and processes of eclogitisation in the UHP region of western Norway. *Journal of Metamorphic Geology*, **19,** 609–625.

Waters, D. J. & Martin, H. N., 1993. Geobarometry of phengite-bearing eclogites. *Terra Abstracts*, **5,** 410–411.

Zhang, R. Y. & Liou, J. G., 2000. Exsolution lamellae in minerals from ultrahigh-pressure rocks. In: *Ultrahigh-pressure Metamorphism and Geodynamics in Collision-type Orogenic Belts, International Lithosphere Project International Book Series* (eds Ernst, W. G. & Liou, J. G.), pp. 216–228, Bellwether Publishing, Ltd., Columbia, MD, USA.

Zhang, R. Y., Liou, J. G., Ernst, W. G., Coleman, R. G., Sobolev, N. V. & Shatsky, V. S., 1997. Metamorphic evolution of diamond-bearing and associated rocks from the Kokchetav massif, northern Kazakhstan. *Journal of Metamorphic Geology*, **15,** 479–496.

Received 22 April 2004; revision accepted 2 July 2004.